The SERK3 elongated allele defines a role for BIR ectodomains in brassinosteroid signalling

Hohmann, Ulrich; Nicolet, Joël; Moretti, Andréa; Hothorn, Ludwig A.; Hothorn, Michael

The SERK3 *elongated* allele defines a role for BIR ectodomains in brassinosteroid signaling.

Author manuscript: published in Nat Plants. 2018 Jun;4(6):345-351. doi: 10.1038/s41477-018-0150-9. Epub 2018 May 7.

Ulrich Hohmann[a], Joël Nicolet[a], Andrea Moretti[a], Ludwig A. Hothorn[b,#], Michael Hothorn[a,1]

[a]Structural Plant Biology Laboratory, Department of Botany and Plant Biology, University of Geneva, Switzerland

[b]Institute of Biostatistics, Leibniz University, Hannover, Germany

[#]retired

Corresponding Author

[1]To whom correspondence may be addressed. Email: michael.hothorn@unige.ch

Keywords: brassinosteroid signaling, membrane receptor kinase, protein kinase, pseudokinase, leucine-rich repeat domain, receptor activation, protein inhibitor.

The leucine-rich repeat receptor kinase (LRR-RK) BRI1 requires a shape-complementary SERK co-receptor for brassinosteroid sensing and receptor activation[1]. Interface mutations that weaken the interaction between receptor and co-receptor *in vitro* reduce brassinosteroid signaling responses[2]. The SERK3 elongated (*elg*) allele[3–5] maps to the complex interface and shows enhanced brassinosteroid signaling, but surprisingly no tighter binding to the BRI1 ectodomain *in vitro*. Here, we report that rather than promoting the interaction with BRI1, the *elg* mutation disrupts the ability of the co-receptor to interact with the ectodomains of BIR receptor pseudokinases, negative regulators of LRR-RK signaling[6]. A conserved lateral surface patch in BIR LRR domains is required for targeting SERK co-receptors and the *elg* allele maps to the core of the complex interface in a 1.25 Å BIR3 – SERK1 structure. Collectively, our structural, quantitative biochemical and genetic analyses suggest that brassinosteroid signaling complex formation is negatively regulated by BIR receptor ectodomains.

The LRR-RK BRASSINOSTEROID INSENSITIVE 1 (BRI1) is the major receptor for growth-promoting steroid hormones in plants[7,8] and binds brassinosteroids (BRs) including the potent brassinolide (BL) with its LRR ectodomain[9,10]. Ligand-associated BRI1 can interact with the LRR domain of a SOMATIC EMBRYOGENESIS RECEPTOR KINASE (SERK) co-receptor kinase, which completes the steroid binding site[1,11]. Heterodimerisation of the receptor and co-receptor LRR domains at the cell surface enables the kinase domains of BRI1 and SERK to trans-phosphorylate each other, allowing BRI1 to activate the cytoplasmic side of the brassinosteroid signaling cascade[12–14]. Mutations in the BRI1 – SERK complex interface that reduce binding between the receptor and co-receptor ectodomains *in vitro*, weaken the interactions of the full-length proteins *in planta* and consequently result in BR loss-of-function phenotypes[2]. Previously, two gain-of-function mutations have been reported for the BR signaling complex: the BRI1 *sud1* allele stabilizes the steroid binding site of the receptor[15,1]. A similar phenotype is observed with the *elg* mutant[5], originally identified as a suppressor of *ga4*, a gibberellic acid biosynthetic enzyme[3]. SERK3^{D122} is replaced by an asparagine residue in *elg* mutant plants[4] and Asn122 maps to the constitutive BRI1 – SERK3 complex interface outside the steroid binding pocket[1,2,11] (Fig. 1a). In BRI1 – SERK complex structures, SERK3^{D122} stabilizes the conformation of SERK3^{R146}, which in turn makes polar contacts with BRI1^{E749} [1,2,9] (Fig. 1a). Mutation of the corresponding Asp128 to asparagine in rice SERK2 alters these interactions[16]. SERK3^{D122} positions SERK3^{E98} for interaction with BRI1^{T750}, which is found replaced by isoleucine in *bri1-102* loss-of-function mutants[17] (Fig. 1a). Taken together, SERK3^{D122} is in contact with several residues critically involved in BR signaling complex formation.

We complemented a *serk1-1 serk3-1* double mutant with 6xHA-tagged wild-type or SERK3 mutant genomic constructs under the control of the SERK3 promoter. We could recapitulate the gain-of-function phenotype of $SERK3^{D122N}$ plants in quantitative hypocotyl growth assays[5] and replacing $SERK3^{D122}$ with alanine resulted in an even stronger BR signaling phenotype (Fig. 1b,c Supplementary Figs. 1-3, Supplementary Table 1). We produced $SERK3^{D122N}$ and $SERK3^{D122A}$ LRR domains by secreted expression in insect cells and characterized their interaction with the BRI1 ectodomain in grating-coupled interferometry (GCI) binding assays[2]. The binding kinetics reveal that wild-type and mutant SERK3 LRR domains bind BRI1 with similar association rates (k_a) (Fig. 1d). $SERK3^{D122A}$ but not $SERK3^{D122N}$ has a slower dissociation rate (k_d) from the receptor, and consequently a slightly lower dissociation constant (K_D). Overall, the only moderately altered binding kinetics for wild-type vs. mutant SERK3 ectodomains cannot rationalize their gain-of-function phenotype *in planta* (Fig. 1b-d).

Recently, the BRI1-ASSOCIATED-KINASE1 INTERACTING KINASE 3 (BIR3) has been reported as a negative regulator of BR signaling in Arabidopsis[6]. Ectopic overexpression of BIR3 results in BR loss-of-function phenotypes including BL insensitivity and reduced BRI1-EMS-SUPPRESSOR 1 (BES1) dephosphorylation[6]. The cytosolic pseudokinase domains of BIR2 and BIR3 bind the SERK3 kinase domain in yeast-2-hybrid assays and the full-length proteins interact *in planta*[6,18]. We hypothesized that also the highly conserved BIR ectodomains may contribute to BIR3 – SERK3 complex formation. Indeed, we found that the recombinantly purified BIR3 LRR domain binds SERK3 with a K_D of ~1 μM and with 1:1 stoichiometry (N) in isothermal titration calorimetry (ITC) experiments (Fig. 2a). No binding was detected between the BIR3 and BRI1 ectodomains (Fig. 2a). The BIR3 and BIR2 ectodomains interact with SERK1-3 with similar binding affinities *in vitro* (K_D ranges from ~1 to ~3 μM) (Fig 2a). Ma et al. reported binding affinities of SERK3 vs. BIR1-4 ranging from ~1 to ~10 μM[19]. The very similar biochemical properties of different BIR and SERK ectodomains allowed us to use different protein isoforms for our various biochemical and structural investigations described below. It is however of note that *bir3* but not *bir2-1* or *bir2-3* mutant plants display a weak BR gain-of-function signaling phenotype (Fig. 2c, Supplementary Figs. 2, 5, Supplementary Table 1). SERK – BIR complex formation is likely driven by their extracellular LRR domains, as we could not observe detectable binding of the cytoplasmic (pseudo)kinase domains in ITC assays (Supplementary Fig. 4).

We next tested if the *elg* mutation could modulate the interaction between BIRs and SERK3. Indeed, the $SERK3^{D122N}$ mutant shows ~4-fold reduced binding to BIR3 and ~8-fold reduced binding to BIR2 (Fig. 2a,b). Due to its low expression yield, the $SERK3^{D122A}$ mutant (Fig. 1) could not be assayed by ITC. Together, our experiments suggest that $SERK3^{D122}$ maps to the interface of

different SERK3 – BIR complexes and that interactions between interface residues may be compromised in the *elg* mutant background.

To gain insight into the BIR targeting mechanism, we sought to determine a crystal structure of BIR3 but did not succeed in obtaining diffraction quality crystals. Crystals of the related BIR2 ectodomain (residues 29-221, ~60% sequence identity with BIR3) diffracted to 1.9 Å resolution (Supplementary Table 2). BIR2 contains five LRRs and shows a high degree of structural conservation with SERKs (r.m.s.d is ~1.5 Å comparing 175 corresponding C_α atoms in BIR2 and SERK1) with the exception of a protruding loop in the N-terminal capping domain of BIR2 (magenta in Fig. 3a). The BIR2 N- and C-terminal caps as well as the LRR core are stabilized by disulfide bridges conserved among the different BIR family members (Fig. 3c, Supplementary Fig. 6). The conserved Asn58 in the BIR2 N-cap is glycosylated in our structure (Fig. 3c, Supplementary Fig. 6). A set of solvent exposed hydrophobic residues including BIR2^{W73} from the protruding loop, BIR2^{F128}, BIR2^{F152} and BIR2^{R176} form a lateral surface patch conserved among BIRs from different species, but not in SERK proteins (Figs. 3b,c, Supplementary Fig. 6). This potential interaction surface differs from the central binding platform used by SERKs for targeting ligand-sensing LRR-RKs (Fig. 3c)[2,14]. We generated several point-mutations in the respective surface areas and assayed the mutant proteins vs. SERK3 in ITC assays. BIR2^{E84R} and BIR2^{V157D} originating from the central LRR groove still bind SERK3, suggesting that this interaction platform is not used by BIRs to target SERKs (Figs. 3c,d). Mutation of BIR2^{W73} from the protruding N-cap loop to alanine weakens the interaction with SERK3 and replacing BIR2^{F152} or BIR2^{R176} from the lateral surface patch with alanine disrupts binding (Figs. 3c,d). Thus, the unique N-cap loop and the lateral surface patch in the LRR domain of BIR2 are involved in the interaction with SERK3.

To understand how BIRs target the central, *elg*-containing surface in SERKs, we performed crystallization trials for various BIR – SERK ectodomain combinations. We obtained crystals for BIR3 – SERK1 and BIR3 – SERK2 complexes diffracting to 1.25 Å and 2.2 Å resolution, respectively (Supplementary Table 2). Our crystals contain a fully glycosylated BIR3 – SERK1 heterodimer in the asymmetric unit, consistent with the in solution behavior of the complex (Figs. 4a, Supplementary Fig. 7). Most surface areas of the SERK1 LRR domain are shielded by carbohydrate, except for the central interaction surface used to, for example, bind the BRI1 and HAESA ligand-sensing LRR-RKs[1,2,9,20]. Structural superposition of our BIR3 – SERK1 and BIR3 – SERK2 complexes reveals that BIRs have a conserved SERK binding mode (Supplementary Fig. 8A, r.m.s.d. is ~1.8 Å comparing 316 corresponding C_α atoms), rationalizing their similar complex dissociation constants (Fig. 2a,b). Comparing the BIR3 – SERK1 complex with structures of the isolated SERK1 and BIR2 ectodomains reveals no major conformational rearrangements in BIRs and SERKs upon complex formation, with the exception of the protruding loop containing BIR2^{W73}

or the corresponding Trp67 in BIR3 (Supplementary Fig. 8b). In the complex structure, BIR3 establishes a network of hydrophobic and polar interactions with the SERK1 C-terminal cap and with the two C-terminal LRRs (total buried complex surface area is ~1,400 Å^2 as calculated with the program DSSP[21]) (Fig. 4a). Several polar contacts are mediated by water molecules. The tip of the BIR3 protruding N-cap loop is in direct contact with the SERK1 *elg* surface (Fig. 4b). SERK residues Asp122 (numbering corresponds to SERK3 throughout) and the neighboring Tyr124 together coordinate a water molecule, which in turn hydrogen bonds with BIR3^{E69} in the protruding loop tip (Fig. 4b). The neighboring Tyr100 establishes an additional hydrogen bond with BIR3^{E69} and the remaining loop tip residues BIR3^{N68} and BIR3^{K70} form similar interaction with SERK residues Asn148 and Asn77, respectively (Fig. 4b). Importantly, mutation of SERK Tyr100 or Tyr124 to alanine reduces BIR2 binding (Fig. 4b,d).

An additional set of hydrophobic contacts involving BIR3^{W67} (corresponds to BIR2^{W73} analyzed in Fig. 3c,d), BIR3^{I75}, BIR3^{Y122}, BIR3^{V124} and BIR3^{F146} (corresponds to BIR2^{F152}, see Fig. 3c,d) and SERK residues Val168, Ile192, Pro191 are dominating the interactions between the BIR3 and SERK1 C-terminal halves (Fig. 4a,c). BIR3^{R170}, the corresponding mutation in BIR2^{R176} to alanine disrupts complex formation with SERK3 (Fig. 3d), forms hydrogen bonds with backbone atoms in the SERK1 C-cap and other polar contacts are mediated by water molecules (Fig. 4c). Taken together, BIR3 targets the central LRR surface of SERKs normally used for the interaction with ligand-sensing LRR-RKs. The unique protruding loop in BIRs directly contacts the *elg* surface patch, rationalizing the reduced binding of SERK3^{D122N} to BIR ectodomains *in vitro* (Fig. 2a,b).

We next tested if the SERK – BIR LRR domain complex interface controls association of the full-length proteins *in planta*. We found that wild-type SERK3 associated with BIR3 in co-immunoprecipitation experiments (Fig. 4f), as shown previously[6]. The SERK3^{D122N}, SERK3^{D122A}, SERK3^{Y100A}, SERK3^{Y124A} mutants, all of which show reduced binding to isolated BIR LRR domains *in vitro*, consistently show reduced interaction with BIR3 *in vivo* (Fig. 4f). SERK3^{F60} lies outside the SERK – BIR complex interface, but forms part of the BRI1 – SERK steroid binding pocket[1,11] and its mutation to alanine disrupts BR complex formation *in vitro* and *in planta*[2]. Consistent with our BIR targeting model, the SERK3^{F60A} mutant shows wild-type binding to BIRs in ITC assays and retains interaction with BIR3 *in vivo* (Fig. 4d,f).

Our biochemical observation that SERKs can form tight heterodimeric complexes with BRI1 or with BIRs using largely overlapping interaction surfaces (Supplementary Fig. 9), prompted us to investigate if the BRI1 and BIR ectodomains could compete for SERK binding. We performed analytical size-exclusion chromatography experiments with the isolated BRI1, SERK3 and BIR2 LRR domains and in the presence or absence of the steroid hormone. In our ITC assay (Fig. 2a), we could not detect complex formation between BRI1 and BIR3, and consistently BIR2 was unable to

dissociate an already formed BRI1-BL-SERK3 complex (Fig. 4g). However, BRI1-BL could efficiently compete with BIR2 for SERK3 binding (Fig. 4g), in line with our observation that the experimentally determined stoichiometries, binding affinities and -kinetics for the different complexes are similar (Figs. 1d, 2a).

Taken together, the molecular characterization of the SERK3 *elg* allele has revealed that the BR signaling pathway is under negative regulation by the ectodomain of BIR3. We show that SERK3^{D122N} disrupts BIR but not BRI1 binding and thus exhibits a gain-of-function phenotype (Figs. 1c, 2b). Mutation of the neighboring SERK3^{Y100} and SERK3^{Y124} to alanine strongly decreases BIR binding, but only SERK3^{Y124A} retains the ability to bind BRI1 – BL with high affinity (Fig. 4d-f). Consistently, SERK3^{Y124A}, but not SERK3^{Y100A} or SERK3$^{Y100A/Y124A}$ displays a statistically significant gain-of-function phenotype in hypocotyl growth assays (Fig. 1b,c). The BR-specific nature of the *elg* allele may thus be related to its ability to bind BRI1, but not other SERK3-dependent LRR-RKs with high affinity[5]. Indeed, we find that SERK3^{D122N} and SERK3^{D122A} mutant proteins bind the SERK-dependent peptide hormone receptor kinase HAESA with drastically reduced affinity (Supplementary Fig. 10). The *elg* and *bir3* phenotypes and our quantitative biochemical assays reveal that BRI1 and BIRs can compete for binding to SERKs, with BRI1 being able to out-compete BIRs in the presence of BL. We speculate that this negative regulation of SERKs by BIR proteins may allow for sharper signal transitions, with signaling competent BR complexes forming only in response to significant changes in BR concentration.

Specific physiological functions have been genetically assigned to the different BIR family members in Arabidopsis: BIR1, a catalytically active protein kinase, specifically inhibits SERK3 co-receptor function in immunity and cell death, with *bir1* loss-of-function mutants showing constitutive defense responses associated with a severe growth phenotype[22,23,19]. BIR2 and BIR3 are additional SERK3 interactors and both proteins are pseudokinases[6,18,24]. Different *bir2* knock-down lines show altered immune responses but no BR signaling phenotype, while *bir3* loss- and gain-of function mutants affect BR signaling (Fig. 2c)[6,18]. We cannot rationalize these specific functions of the different BIRs at the biochemical level, as all BIR ectodomains tested bind various SERK proteins with similar dissociation constants (Fig. 2a), in agreement with a recent study on the role of BIR1 in FLS2-mediated immune signaling[19]. This behavior of BIR proteins is reminiscent of SERKs, which also are largely promiscuous at the biochemical level, but which show partly specific, partly overlapping functions in plant growth, development and immunity[14]. While BIR ectodomains and not their cytosolic kinase domains allow for high affinity SERK binding (Figs. 2-4, Supplementary Fig. 4), BIR signaling specificity may be encoded in their cytosolic domains, as seen with ligand-sensing LRR-RKs[2,25]. In line with this, specific BIR adapter proteins have been reported[26,27], which could allow for the targeting of BIR family members to specific membrane

(nano)-domains[28], and which could help to create specific signaling outputs in the cytosol[26]. While we cannot rule out a redundant function for BIR receptor kinases, the fact that the *bir3-2* mutant does not phenocopy *elg* plants (Figs. 1b, 2c), suggests that other negative regulators of BR signaling complexes remain to be discovered.

Methods

See Supplementary Information for complete details.

Reproducibility

At least two independent experiments were performed for all biochemical assays (ITC, GCI and gel filtration assays). Co-IP, hypocotyl growth assays and western blots were performed at least three times, all with similar outcome.

Protein expression and purification of LRR ectodomains

SERK2$^{1-220}$, SERK3$^{1-220}$ and BRI1$^{1-788}$ were amplified from *A. thaliana* cDNA and BIR1$^{1-219}$, BIR2$^{1-222,}$ BIR3$^{1-213}$ from *A. thaliana* genomic DNA. BIR2$^{1-222}$ was in addition obtained codon-optimized for expression in *Trichoplusia ni* (strain Tnao38), SERK1$^{24-213}$ as well as HAESA$^{20-620}$ were obtained codon optimized and fused to an azurocidin signal peptide; all constructs were cloned in a modified pFastBac vector (Geneva Biotech), containing a TEV (tobacco etch virus protease) cleavable C-terminal StrepII-9xHis tag. Mutations were created using site directed mutagenesis (Supplementary Table 3). Tnao38[29] cells were infected with a multiplicity of infection (MOI) of 1 for SERKs or 3 for BRI1, HAESA and BIRs at a density of 2x10^{6}cells/ml and incubated 26 h at 28 °C and 48 h at 22 °C. Subsequently the secreted proteins were purified from the supernatant by Ni^{2+} (HisTrap excel; GE Healthcare; equilibrated in 25 mM KP_i pH 7.8, 500 mM NaCl) and StrepII (Strep-Tactin Superflow high capacity; IBA; equilibrated in 25 mM Tris pH 8.0, 250 mM NaCl, 1 mM EDTA) affinity chromatography. The purity of the preparations was further improved by size-exclusion chromatography on either a Superdex 200 increase 10/300 GL, HiLoad 16/600 Superdex 200 pg or HiLoad 26/600 Superdex 200 pg column (GE Healthcare), equilibrated in 20 mM sodium citrate pH 5.0, 150 mM NaCl. Molar protein concentrations for BIR2, BIR3, SERK1, SERK3, BRI1 and HAESA were calculated using their molar extinction coefficient and molecular weights of 23.4, 24.0, 25.2, 27.4, 105.0, 74.9 kDa, respectively (as determined by MALDI-TOF mass spectrometry).

Grating coupled interferometry (GCI)

The Creoptix WAVE system (Creoptix AG, Switzerland), a label-free surface biosensor[30] was used to perform GCI experiments. All experiments were performed on 2PCP WAVEchips (quasi-planar

polycarboxylate surface; Creoptix AG, Switzerland). After a borate buffer conditioning (100 mM sodium borate pH 9.0, 1 M NaCl; Xantec, Germany) the respective LRR ectodomain was immobilized on the chip surface using standard amine-coupling: 7 min activation (1:1 mix of 400 mM N-(3-dimethylaminopropyl)-N'-ethylcarbodiimide hydrochloride and 100 mM N-hydroxysuccinimide [both Xantec, Germany]), injection of the LRR domain (10 to 40 µg/ml) in 10 mM sodium acetate pH 5.0 (Sigma, Germany) until the desired density was reached, passivation of the surface (0.5% BSA [Roche, Switzerland] in 10mM sodium acetate pH 5.0) and final quenching with 1 M ethanolamine pH 8.0 for 7 min (Xantec, Germany). For a typical experiment, SERK3 was injected in a 1:2 dilution series (starting from 2 µM) in 20mM citrate pH 5.0, 250mM NaCl at 25°C. Blank injections were used for double referencing and a DMSO calibration curve for bulk correction. Analysis and correction of the obtained data was performed using the Creoptix WAVEcontrol software (applied corrections: X and Y offset, DMSO calibration, double referencing) and a one-to-one binding model with bulk correction was used to fit all experiments.

Isothermal titration calorimetry (ITC)

All ITC experiments were performed on a Nano ITC (TA Instruments) with a 1.0 ml standard cell and a 250 µl titration syringe at 25 °C. Proteins were gelfiltrated or dialyzed into ITC buffer (20 mM sodium citrate pH 5.0, 150 mM NaCl for LRR domains / 20 mM Hepes pH 7.5, 150 mM NaCl, 1 mM $MgCl_2$, 0.5 mM TCEP for kinase domains) prior to all experiments. For a typical ectodomain experiment, 16 µl of BIR (at ~400 µM) was injected into ~40 µM SERK protein in the cell at 150 s intervals (15 injections). Experiments with the kinase domains were performed by injecting 10 µl of BIR2 or BRI1 cytosolic domain at ~200 µM into ~20 µM of SERK3 kinase domain in the cell at 150s intervals (25 injections). Data was corrected for the dilution heat and analyzed using NanoAnalyze program (version 3.5) as provided by the manufacturer.

Plant protein extraction and immunoprecipitation

Surface-sterilized and stratified seeds were plated on ½ MS, 0.8 % agar plates and grown for ~14 d. Seedlings were frozen in liquid N_2, ground to fine powder using mortar and pestel (1 g per sample) and resuspended in 3 ml of ice cold extraction buffer (50 mM Bis Tris pH 7.0, 150mM NaCl, 10 % (v/v) glycerol, 1 % Triton X-100, 5 mM DTT, protease inhibitor cocktail (P9599, Sigma). After gentle agitation for 1 h at 4 °C, samples were centrifuged for 30 min at 4 °C and 16,000 g; the supernatant was transferred to a fresh tube and the protein concentration measured using a Bradford assay. 20 mg of total protein in a volume of 5 ml were incubated with 50 µl of anti-HA superparamagnetic MicroBeads (Miltenyi Biotec) for 1 h at 4 °C with agitation for each co-immunoprecipitation (Co-IP). The beads were then collected using µMACS Columns (Miltenyi

Biotec), washed 4 times with 1 ml of cold extraction buffer and proteins were eluted in 20+20 µl of extraction buffer at 95 °C. Samples were separated on 10 % SDS-PAGE gels; In the subsequent western blots SERK3:6HA was detected using anti-HA antibody coupled to horse radish peroxidase (HRP, Miltenyi Biotec) at 1:5,000 dilution, while BIR3 was detected using a polyclonal BIR3 antibody[6] at 1:500 dilution followed a secondary anti-rabbit HRP antibody (1:10,000, Calbiochem #401353). Co-immunoprecipitation experiments were repeated two times, with similar outcome.

Analytical size exclusion chromatography

Gel filtration experiments were performed using a Superdex 200 Increase 10/300 GL column (GE Healthcare) pre-equilibrated in either 20 mM sodium citrate pH 5.0, 150 mM NaCl for LRR domain interaction assays, or with 20 mM Hepes pH 7.5, 150 mM NaCl, 1 mM $MgCl_2$, 0.5 mM TCEP for cytoplasmic domain oligomeric state analysis. 500 µl of the respective protein (0.2 mg/mL) was loaded sequentially onto the column and elution at 0.75 ml/min was monitored by ultraviolet absorbance at 280 nm. BL concentration was 1 µM in the BRI1 – BL - SERK3 complex sample prior to loading.

Data availability statement

Materials used in this study and data generated are available from the corresponding author upon request. Crystallographic coordinates and structure factors have been deposited with the Protein Data Bank (http://rcsb.org) with accession codes 6FG7 (BIR2), 6FG8 (BIR3 – SERK1) and 6G3W (BIR3-SERK2).

Acknowledgements

We thank B. Kemmerling for kindly providing us with BIR2 and BIR3 polyclonal antibodies, N. Geldner for providing seeds, and the staff at beam line PXIII of the Swiss Light Source, Villigen, Switzerland for technical assistance during data collection, J. Santiago for providing the SERK2 expression plasmid, and K. Lau for help with preparing figures. This work was supported by grant 31003A_176237 from the Swiss National Science Foundation and by an International Research Scholar Award from the Howard Hughes Medical Institute (to MH).

Contributions

U.H., and M.H. designed research; U.H. performed most of the experiments; J.N. contributed to generation and characterization of transgenic lines and A.M. conducted experiments on the cytoplasmic domains; U.H., A.M., L.A.H., and M.H. analyzed data; and U.H. and M.H. wrote the manuscript.

Figure legends

Fig. 1: SERK3 *elg* is a gain of function mutation *in vivo* but not *in vitro.*

a, Ribbon diagram of the *elg*-containing complex interface, as seen in the BRI1 – BL – SERK1 structure (PDB-ID 4LSX[1]). BRI1 and SERK are depicted in blue and orange, respectively, selected residues are shown in ball-and-stick representation with the elg residue Asp122 highlighted in yellow. Polar interactions are shown as dotted lines. SERK residue numbering is according to the SERK3 sequence throughout.

b, Hypocotyl growth assay of dark grown seedlings in the pre- and absence of the BR biosynthesis inhibitor brassinazole (BRZ). The BRZ hypersensitivity seen in the *serk1-1 serk3-1* mutant is complemented by the expression of $SERK3^{WT}$ (Col-0 is the untransformed wild-type). Shown alongside is the quantification of the data with relative inhibition plotted together with lower and upper confidence intervals. For each sample (i.e. genotype and treated or untreated) n=50 biologically independent hypocotyls, coming from 5 different ½MS plates, were measured.

c, Western blot using an HA antibody against SERK3:HA from plant material shown in (**b**). A Ponceau loading control is shown beneath.

d, Binding kinetics for SERK3, $SERK3^{D122A}$ and $SERK3^{D122N}$ (*elg*) vs. BRI1 in the presence of BL obtained from grating-coupled interferometry (GCI) experiments. Sensograms with recorded data are shown in red with the respective fits in black, and include table summaries of the corresponding association rate constant (k_a), dissociation rate constant (k_d) and dissociation constant K_D.

Fig. 2: BIR ectodomains interact with different SERK co-receptors *in vitro.*

a,b, Isothermal titration calorimetry (ITC) experiments of BIR2 and BIR3 LRR domains vs. (**a**) wild-type SERK ectodomains and (**b**) vs. the $SERK3^{D122N}$ mutant ectodomain and including table summaries for dissociation constants (K_D,) and binding stoichiometries (N) (± fitting error; n.d.: no detectable binding).

c, Hypocotyl growth assay in the pre- and absence of BRZ (compare Fig. 1b). Relative inhibition together with upper and lower confidence intervals are shown alongside; Col-0 and *serk1-1 serk3-1* are the same as shown in Fig. 1b. For each sample (i.e. genotype and treated or untreated) n=50 biologically independent hypocotyls, coming from 5 different ½MS plates, were measured.

Fig. 3: The BIR2 ectodomain adopts a SERK-like fold with an additional lateral protein interaction interface.

a, Structural superposition of the isolated BIR2 and SERK1 (PDB-ID 4LSC[1]) ectodomains (r.m.s.d. is ~1.5 Å comparing 175 corresponding C_α atoms). C_α traces of SERK1 (orange) and BIR2 (blue) are shown; the unique, protruding BIR2 N-terminal cap loop region is highlighted in magenta.

b, Surface representation of the BIR2 ectodomain, gradient colored according to the amino-acid sequence conservation of BIR proteins from different species (compare Fig. S4).
c, The extracellular BIR2 domain consists of five LRRs with N- and C-terminal capping domains and a lateral protein interaction interface. Shown is a ribbon diagram of the BIR2 LRR domain (in blue), the four disulfide bonds are highlighted in green, selected residues in the lateral interface are in yellow, residues in the LRR central groove in cyan, and the N-glycan moiety in gray (all in ball-and-sticks representation).
d, ITC experiments of BIR2 ectodomain mutants vs. the extracellular domain of SERK3 with table summaries alongside.

Fig. 4: A BIR3-SERK1 complex structure provides a mechanism for SERK gain-of-function mutations.
a, Structure of the BIR3 – SERK1 ectodomain complex, with BIR3 shown in blue and SERK1 in orange and with N-glycans highlighted in ball-and-sticks representation.
b,c, Detailed views of the BIR3 – SERK1 complex interface. Selected interface residues are shown in ball-and-sticks representation with the mutationally analyzed Tyr100, Asp122 and Y214 highlighted in yellow. Water molecules are depicted as red spheres, polar interactions are shown as dotted lines.
d, ITC binding experiments of BIR2 vs. different SERK3 mutants.
e, Binding kinetics of $SERK3^{Y100A}$ and $SERK3^{Y124A}$ to BL-associated BRI1 derived from GCI experiments. Fitted kinetic parameters are shown alongside.
f, Co-immunoprecipitation (Co-IP) experiment using different SERK3 lines vs. BIR3. Input western-blots and a Ponceau stained membrane are shown alongside.
g, Size-exclusion chromatography experiments using the BIR2, SERK3, BRI1 ectodomains. BIR2 forms no complex with BRI1 (red line), and is not able to dissociate a preformed BRI1 – BL – SERK3 complex (gray line). However, incubation of a preformed BIR2 – SERK3 complex with BRI1 – BL reveals formation of BRI1 – BL – SERK3 complexes (black line), suggesting that BRI1 – BL can compete with BIR2 for SERK3 binding. Void (v_0) volume and total volume (v_t) are shown, together with elution volumes for molecular mass standards (Al, Aldolase, 158,000 Da; Ov, Ovalbumin, 44,000 Da; CA, Carbonic anhydrase, 29,000 Da). Peak fractions were analyzed by SDS-PAGE.

References

1. Santiago, J., Henzler, C. & Hothorn, M. Molecular mechanism for plant steroid receptor activation by somatic embryogenesis co-receptor kinases. *Science* **341,** 889–892 (2013).
2. Hohmann, U. *et al.* Mechanistic basis for the activation of plant membrane receptor kinases by SERK-family coreceptors. *Proc. Natl. Acad. Sci.* **115,** 3488–3493 (2018).
3. Halliday, K., Devlin, P. F., Whitelam, G. C., Hanhart, C. & Koornneef, M. The ELONGATED gene of Arabidopsis acts independently of light and gibberellins in the control of elongation growth. *Plant J.* **9,** 305–312 (1996).
4. Whippo, C. W. & Hangarter, R. P. A brassinosteroid-hypersensitive mutant of BAK1 indicates that a convergence of photomorphogenic and hormonal signaling modulates phototropism. *Plant Physiol.* **139,** 448–457 (2005).
5. Jaillais, Y., Belkhadir, Y., Balsemão-Pires, E., Dangl, J. L. & Chory, J. Extracellular leucine-rich repeats as a platform for receptor/coreceptor complex formation. *Proc. Natl. Acad. Sci. U. S. A.* **108,** 8503–8507 (2011).
6. Imkampe, J. *et al.* The Arabidopsis Leucine-Rich Repeat Receptor Kinase BIR3 Negatively Regulates BAK1 Receptor Complex Formation and Stabilizes BAK1. *Plant Cell* **29,** 2285–2303 (2017).
7. Clouse, S. D., Langford, M. & McMorris, T. C. A Brassinosteroid-Insensitive Mutant in Arabidopsis thaliana Exhibits Multiple Defects in Growth and Development. *Plant Physiol.* **111,** 671–678 (1996).
8. Li, J. & Chory, J. A putative leucine-rich repeat receptor kinase involved in brassinosteroid signal transduction. *Cell* **90,** 929–938 (1997).
9. Hothorn, M. *et al.* Structural basis of steroid hormone perception by the receptor kinase BRI1. *Nature* **474,** 467–471 (2011).
10. She, J. *et al.* Structural insight into brassinosteroid perception by BRI1. *Nature* **474,** 472–476 (2011).
11. Sun, Y. *et al.* Structure reveals that BAK1 as a co-receptor recognizes the BRI1-bound brassinolide. *Cell Res.* **23,** 1326–1329 (2013).

12. Wang, X. *et al.* Sequential transphosphorylation of the BRI1/BAK1 receptor kinase complex impacts early events in brassinosteroid signaling. *Dev. Cell* **15,** 220–235 (2008).
13. Bojar, D. *et al.* Crystal structures of the phosphorylated BRI1 kinase domain and implications for brassinosteroid signal initiation. *Plant J.* **78,** 31–43 (2014).
14. Hohmann, U., Lau, K. & Hothorn, M. The Structural Basis of Ligand Perception and Signal Activation by Receptor Kinases. *Annu. Rev. Plant Biol.* **68,** 109–137 (2017).
15. Belkhadir, Y. *et al.* Brassinosteroids modulate the efficiency of plant immune responses to microbe-associated molecular patterns. *Proc. Natl. Acad. Sci. U. S. A.* **109,** 297–302 (2012).
16. McAndrew, R. *et al.* Structure of the OsSERK2 leucine-rich repeat extracellular domain. *Acta Crystallogr. D Biol. Crystallogr.* **70,** 3080–3086 (2014).
17. Friedrichsen, D. M., Joazeiro, C. A. P., Li, J., Hunter, T. & Chory, J. Brassinosteroid-Insensitive-1 Is a Ubiquitously Expressed Leucine-Rich Repeat Receptor Serine/Threonine Kinase. *Plant Physiol.* **123,** 1247–1256 (2000).
18. Halter, T. *et al.* The Leucine-Rich Repeat Receptor Kinase BIR2 Is a Negative Regulator of BAK1 in Plant Immunity. *Curr. Biol.* **24,** 134–143 (2014).
19. Ma, C. *et al.* Structural basis for BIR1-mediated negative regulation of plant immunity. *Cell Res.* **27,** 1521–1524 (2017).
20. Santiago, J. *et al.* Mechanistic insight into a peptide hormone signaling complex mediating floral organ abscission. *eLife* **5,** e15075 (2016).
21. Kabsch, W. & Sander, C. Dictionary of protein secondary structure: pattern recognition of hydrogen-bonded and geometrical features. *Biopolymers* **22,** 2577–2637 (1983).
22. Gao, M. *et al.* Regulation of cell death and innate immunity by two receptor-like kinases in Arabidopsis. *Cell Host Microbe* **6,** 34–44 (2009).
23. Liu, Y., Huang, X., Li, M., He, P. & Zhang, Y. Loss-of-function of Arabidopsis receptor-like kinase BIR1 activates cell death and defense responses mediated by BAK1 and SOBIR1. *New Phytol.* **212,** 637–645 (2016).
24. Blaum, B. S. *et al.* Structure of the pseudokinase domain of BIR2, a regulator of BAK1-mediated immune signaling in Arabidopsis. *J. Struct. Biol.* **186,** 112–121 (2014).
25. He, Z. *et al.* Perception of brassinosteroids by the extracellular domain of the receptor kinase BRI1. *Science* **288,** 2360–2363 (2000).

26. Wang, Z., Meng, P., Zhang, X., Ren, D. & Yang, S. BON1 interacts with the protein kinases BIR1 and BAK1 in modulation of temperature-dependent plant growth and cell death in Arabidopsis. *Plant J.* **67,** 1081–1093 (2011).
27. Li, Y., Gou, M., Sun, Q. & Hua, J. Requirement of calcium binding, myristoylation, and protein-protein interaction for the Copine BON1 function in Arabidopsis. *J. Biol. Chem.* **285,** 29884–29891 (2010).
28. Bücherl, C. A. *et al.* Plant immune and growth receptors share common signalling components but localise to distinct plasma membrane nanodomains. *eLife* **6,** (2017).
29. Hashimoto, Y., Zhang, S. & Blissard, G. W. Ao38, a new cell line from eggs of the black witch moth, Ascalapha odorata (Lepidoptera: Noctuidae), is permissive for AcMNPV infection and produces high levels of recombinant proteins. *BMC Biotechnol.* **10,** 50 (2010).
30. Kozma, P., Hamori, A., Cottier, K., Kurunczi, S. & Horvath, R. Grating coupled interferometry for optical sensing. *Appl. Phys. B* **97,** 5–8 (2009).

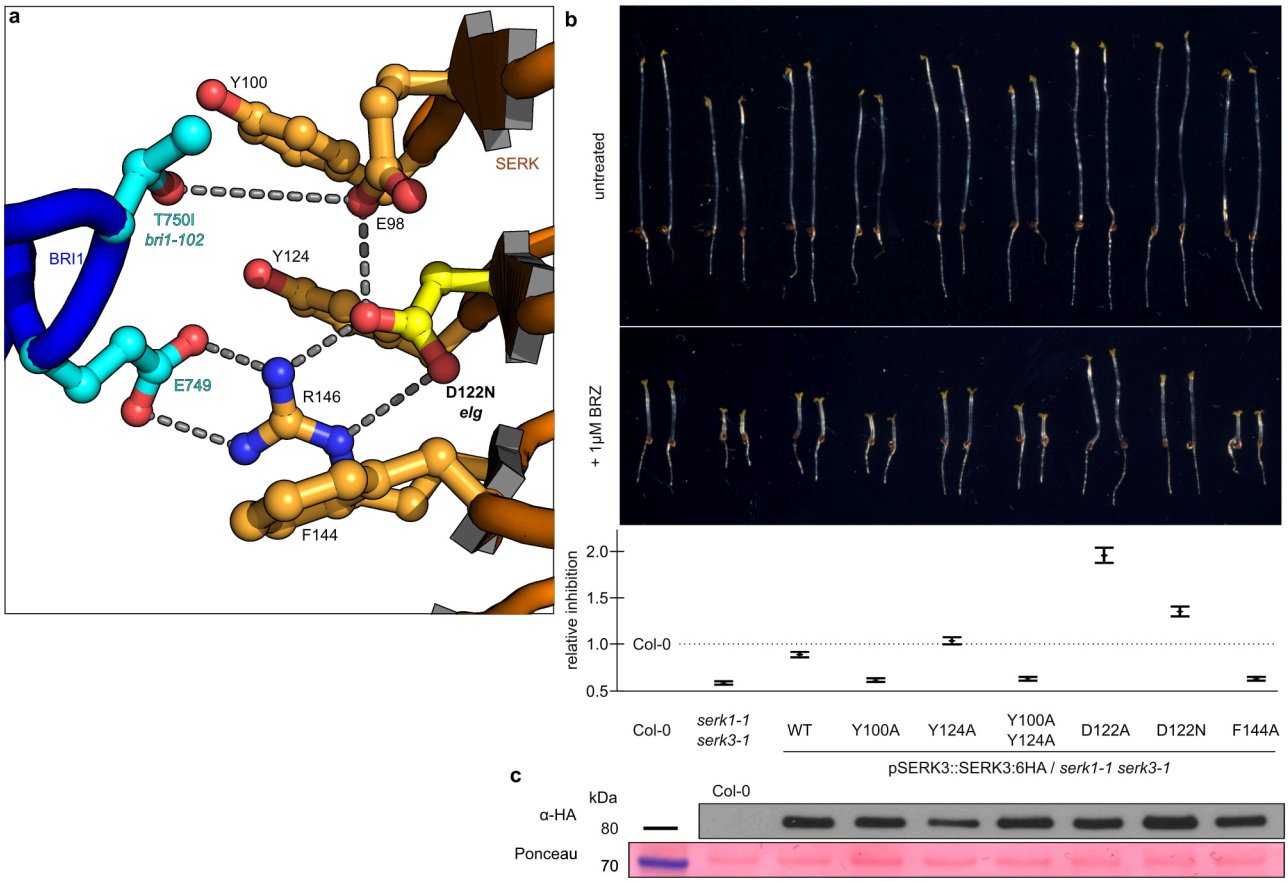
a
Y100
SERK
T750I
bri1-102
BRI1
E98
Y124
E749
R146
D122N
elg
F144
b
untreated
+ 1µM BRZ
relative inhibition
2.0
1.5
1.0
Col-0
0.5
Col-0
serk1-1
serk3-1
WT
Y100A
Y124A
Y100A
Y124A
D122A
D122N
F144A
pSERK3::SERK3:6HA / serk1-1 serk3-1
c
kDa
Col-0
α-HA
80
Ponceau
70
d
SERK3 vs. BRI1+BL
k_a 4.66 x 10^4 M^-1s^-1
k_d 2.41 x 10^-2 s^-1
K_D 0.52 µM
D122A vs. BRI1+BL
k_a 4.40 x 10^4 M^-1s^-1
k_d 6.96 x 10^-3 s^-1
K_D 0.16 µM
D122N vs. BRI1+BL
k_a 6.34 x 10^4 M^-1s^-1
k_d 1.69 x 10^-2 s^-1
K_D 0.27 µM
Surface Mass (pg/mm²)
Time (s)

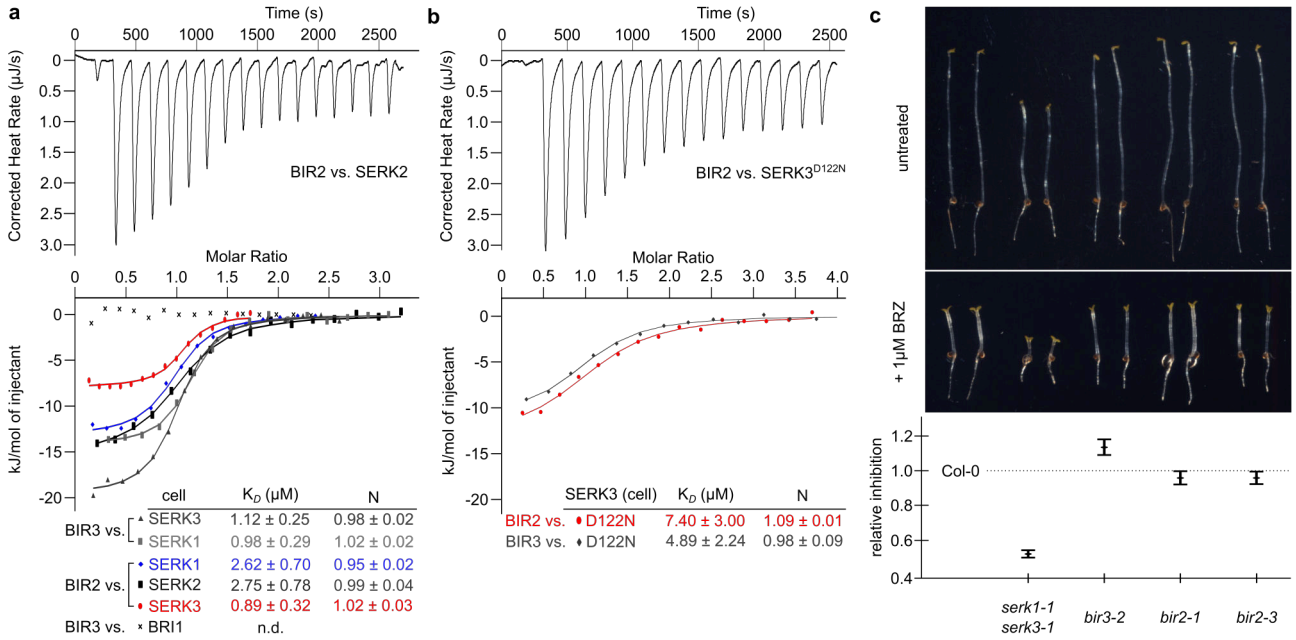
a
Time (s)
Corrected Heat Rate (µJ/s)
BIR2 vs. SERK2
Molar Ratio
kJ/mol of injectant
cell
K_D (µM)
N
BIR3 vs. SERK3 1.12 ± 0.25 0.98 ± 0.02
SERK1 0.98 ± 0.29 1.02 ± 0.02
BIR2 vs. SERK1 2.62 ± 0.70 0.95 ± 0.02
SERK2 2.75 ± 0.78 0.99 ± 0.04
SERK3 0.89 ± 0.32 1.02 ± 0.03
BIR3 vs. BRI1 n.d.
b
Time (s)
Corrected Heat Rate (µJ/s)
BIR2 vs. SERK3D122N
Molar Ratio
kJ/mol of injectant
SERK3 (cell)
K_D (µM)
N
BIR2 vs. D122N 7.40 ± 3.00 1.09 ± 0.01
BIR3 vs. D122N 4.89 ± 2.24 0.98 ± 0.09
c
untreated
+ 1µM BRZ
relative inhibition
Col-0
serk1-1 serk3-1
bir3-2
bir2-1
bir2-3

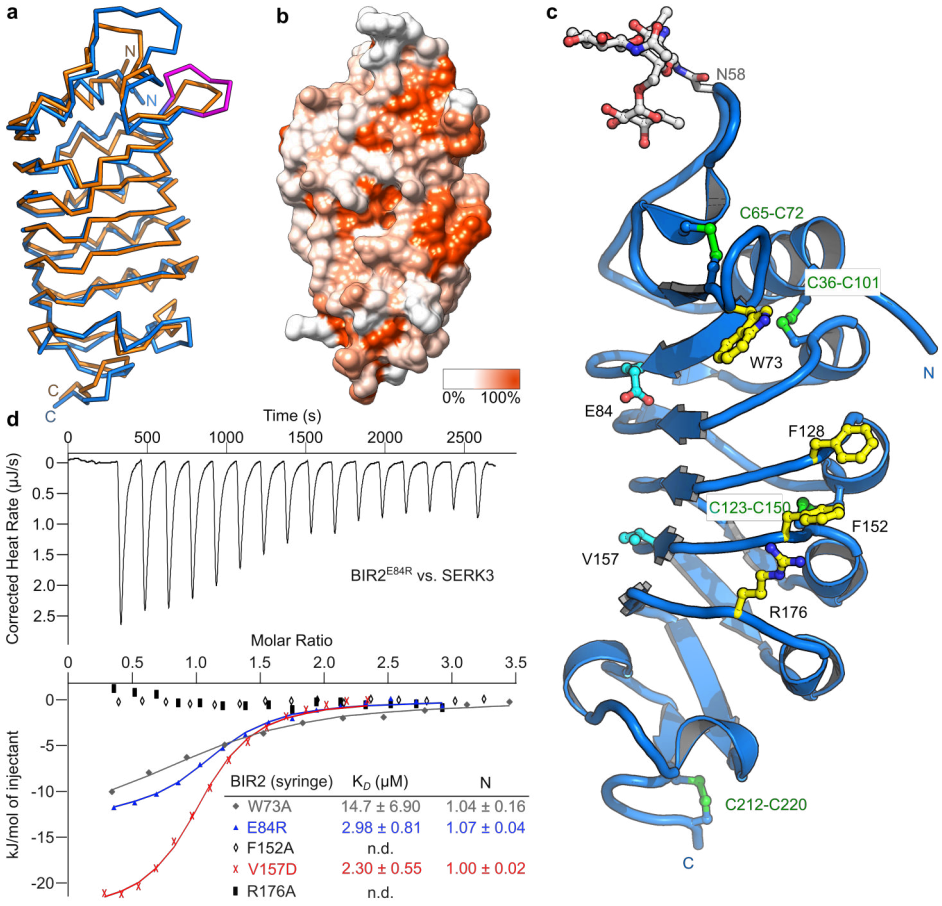
a
N
N
C
C
b
0%
100%
c
N58
C65-C72
C36-C101
W73
N
E84
F128
C123-C150
F152
V157
R176
C212-C220
C
d
Time (s)
0
500
1000
1500
2000
2500
Corrected Heat Rate (µJ/s)
0
0.5
1.0
1.5
2.0
2.5
BIR2E84R vs. SERK3
Molar Ratio
0
0.5
1.0
1.5
2.0
2.5
3.0
3.5
kJ/mol of injectant
0
-5
-10
-15
-20
BIR2 (syringe)
KD (µM)
N
W73A
14.7 ± 6.90
1.04 ± 0.16
E84R
2.98 ± 0.81
1.07 ± 0.04
F152A
n.d.
V157D
2.30 ± 0.55
1.00 ± 0.02
R176A
n.d.

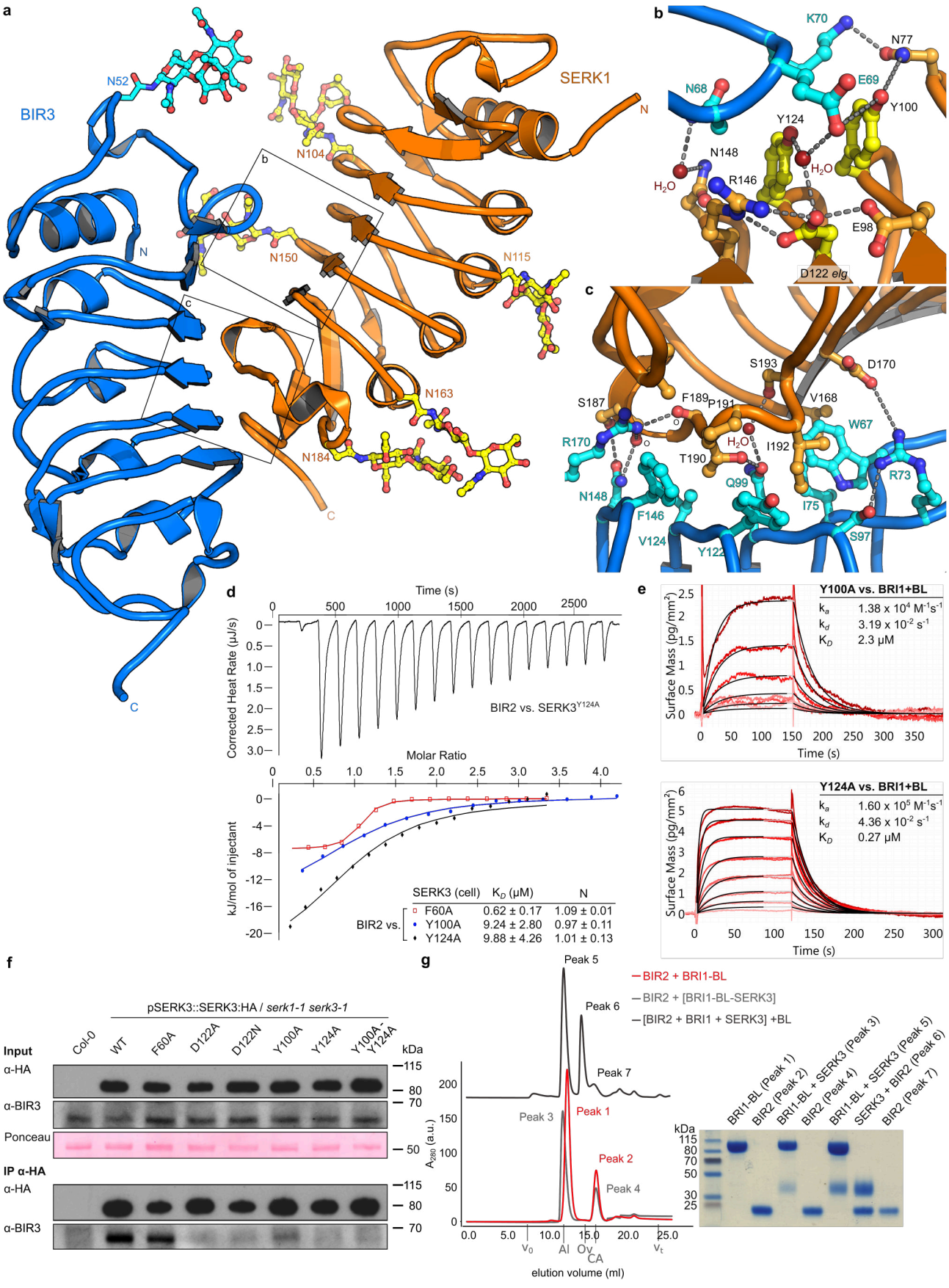
a
BIR3
SERK1
N52
N104
N150
N115
N163
N184
N
C
b
c
b
K70
N77
N68
E69
Y100
Y124
N148
H2O
R146
E98
D122 elg
c
S193
D170
S187
F189
P191
V168
W67
R170
H2O
I192
T190
R73
Q99
N148
I75
F146
V124
S97
Y122
d
Time (s)
Corrected Heat Rate (µJ/s)
BIR2 vs. SERK3Y124A
Molar Ratio
kJ/mol of injectant
SERK3 (cell) KD (µM) N
BIR2 vs. F60A 0.62 ± 0.17 1.09 ± 0.01
Y100A 9.24 ± 2.80 0.97 ± 0.11
Y124A 9.88 ± 4.26 1.01 ± 0.13
e
Y100A vs. BRI1+BL
ka 1.38 x 10^4 M^-1s^-1
kd 3.19 x 10^-2 s^-1
KD 2.3 µM
Surface Mass (pg/mm2)
Time (s)
Y124A vs. BRI1+BL
ka 1.60 x 10^5 M^-1s^-1
kd 4.36 x 10^-2 s^-1
KD 0.27 µM
f
pSERK3::SERK3:HA / serk1-1 serk3-1
Col-0
WT
F60A
D122A
D122N
Y100A
Y124A
Y100A-Y124A
kDa
Input
α-HA
α-BIR3
Ponceau
IP α-HA
α-HA
α-BIR3
115
80
70
50
g
BIR2 + BRI1-BL
BIR2 + [BRI1-BL-SERK3]
[BIR2 + BRI1 + SERK3] +BL
Peak 1
Peak 2
Peak 3
Peak 4
Peak 5
Peak 6
Peak 7
A280 (a.u.)
elution volume (ml)
V0
Al
Ov
CA
Vt
BRI1-BL (Peak 1)
BIR2 (Peak 2)
BRI1-BL + SERK3 (Peak 3)
BIR2 (Peak 4)
BRI1-BL + SERK3 (Peak 5)
SERK3 + BIR2 (Peak 6)
BIR2 (Peak 7)
kDa
115
80
70
50
30
25

Supplementary Methods

Plant material and growth conditions

Genomic *SERK3* was amplified from *Arabidopsis thaliana* (ecotype Col-0), cloned into pDONR221 (ThermoFisher Scientific) and mutations were introduced by site directed mutagenesis (Supplementary Table 3). Constructs were assembled employing multi-site Gateway technology into the binary vector **pH7m34GW** (ThermoFisher Scientific), introduced in the *Agrobacterium tumefaciens* strain pGV2260, and transformed into *Arabidopsis using* the floral dip method[1]. Plants were grown in long day conditions (16 h light) at 21 °C, 50 % humidity and analyzed in homozygous T3 generation. The *bir2-1* (GK_793F12)[2], *bir2-3* (SAIL1288_G07) and *bir3-2* (SALK_116632)[3] T-DNA insertion lines were obtained from the Nottingham Arabidopsis Stock Center (NASC). A *serk1-1* (SALK_044330)[4] *serk3-1* (SALK_034523)[5] double mutant was used as the genetic background for complementation with wild type and mutant *SERK3*.

Hypocotyl growth assay

After surface sterilization with 70 % ethanol, 0.1 % Triton X-100 for 20 min and stratification at 4 °C for 2 days, seeds were plated on ½ MS, 0.8 % agar plates supplemented with either 1 µM brassinazole (BRZ, from a 10 mM stock solution in 100 % DMSO, Tokyo Chemical Industry Co. LTD) or, for the controls, with 0.1 % (v/v) DMSO. After light exposure for 1 h, plates were incubated at 22 °C for 5 d in the dark and subsequently scanned at 600 dpi on a regular flatbed scanner (CanoScan 9000F, Canon). Measurements were taken using FIJI[6] and analyzed with the packages mratios[7] and multcomp[8] as implemented in R[9] (version 3.3.2). We report unadjusted 95% confidence limits for fold-changes instead of p-values[10]. Log-transformed endpoint hypocotyl lengths were analyzed employing a mixed effects model for the ratio of of a given line to the wild-type Col-0 allowing heterogeneous variances. To evaluate the treatment-by-mutant interaction, the 95 % two-sided confidence intervals for the relative inhibition (Col-0: untreated vs. BRZ-treated hypocotyl length)/(any genotype: untreated vs. BRZ-treated hypocotyl length) was calculated for the log-transformed length.

Protein crystallization and data collection

Crystals of the isolated BIR2 ectodomain were grown in sitting drops composed of 0.2 µl of protein solution ($BIR2^{29-222}$ at 9 mg/ml in 20 mM sodium citrate pH 5.0, 150 mM NaCl) and 0.2 µl of 1.8 M sodium malonate pH 4.0. Crystals formed after several months, were cryoprotected in 2.4 M sodium malonate pH 4.0 and were snap frozen in liquid N_2. Native (λ= 1.00 Å) and anomalous (λ= 2.00 Å) datasets were collected from a single crystal at beam line PX-III of the Swiss Light Source, Villigen

(Supplementary Table 2). Crystals of the BIR3$^{25-213}$ – SERK1$^{24-213}$ complex were grown from hanging drops containing 1 µl of protein solution (14 mg/ml in 20 mM sodium citrate pH 5.0, 150 mM NaCl) and crystallization buffer (19% [w/v] PEG 3,350, 1M LiCl, 0.1 M sodium acetate pH 5.5), suspended over 0.6 ml of the latter as reservoir solution. Crystals were cryoprotected by serial transfer in reservoir solution supplemented with a final concentration of 15% (v/v) glycerol. Crystals diffracted up to 1.0 Å at PX-III and due to the beam line geometry, a complete dataset at 1.25 Å was recorded (λ= 1.03 Å, Supplementary Table 2). Crystals of the BIR3$^{25-213}$ – SERK2$^{28-216}$ complex developed in sitting drops containing 0.2 µl protein solution (9 mg/ml in 20 mM sodium citrate pH 5.0, 150 mM NaCl) and crystallization buffer (25 % [w/v] PEG 3,350, 0.2 M $MgCl_2 \cdot 6 H_2O$, 0.1 M Bis Tris pH 6.5). A complete dataset to 2.2 Å was collected at PX-III with λ= 1.00 Å. Data processing and scaling was done with XDS[11] (version: June, 2017).

Crystallographic structure solution and refinement

The BIR2 anomalous dataset was used for experimental phasing using the Single Anomalous Diffraction (SAD) method. Ten consistent sulfur sites were identified using ShelxD[12] and Phenix.hyss[13] and used for site refinement and phasing in Sharp[14] (anomalous phasing power was 0.558 and figure of merit was 0.27 between 44.75 – 3.0 Å). Density modification, 2-fold NCS averaging and phase extension to 1.9 Å in the program Phenix.resolve[15] yielded a readily interpretable electron density map and the structure was completed in alternating cycles of manual building/rebuilding in Coot[16], and restrained TLS refinement in Refmac5[17] (Supplementary Table 2). The structure of the BIR3 – SERK1 complex was solved using the molecular replacement method as implemented in the program Phaser[18], and using the isolated BIR2 and SERK1 (PDB-ID 4LSC[19]) structures as search models. The solution comprises a hetero-dimer in the asymmetric unit and the structure was completed by manual correction in Coot and anisotropic B-factor refinement in Refmac5. The structure of the BIR3 – SERK2 complex was solved using the BIR3 and SERK2 (PDB-ID 4Z61[20]) ectodomains as search models in Phaser. The final solution contains two BIR3-SERK2 heterodimers in the asymmetric unit. Analysis of the refined models with the program Molprobity[21] revealed excellent sterochemistry and no ramachandran outliers for all reported structures. Structural diagrams were made with Pymol (https://sourceforge.net/projects/pymol/) and Chimera[22].

Protein expression and purification of cytoplasmic domains

The cytosolic domain of BIR2 (residues 258-605 or 289-605) was cloned in a modified pET vector (Novagen) providing a TEV cleavable N-terminal 8xHis-StrepII-Thioredoxin tag, constructs were transformed in *E.coli* BL21 (DE3) RIL cells. Protein expression was induced by adding IPTG (0.5

mM final concentration) to cell cultures grown at 37 °C to a OD_{600}= 0.6 and bacteria were harvested after incubation for 18 h at 16 °C. SERK3 (residues 250-615) and BRI1 (residues 814-1196) cytoplasmic domains were cloned in a modified pFastBac vector (Geneva Biotech) with a TEV-cleavable N-terminal 10xHis-2xStrepII tag for expression in insect cells. Proteins were expressed in Tnao38 cells for three days at 28 °C after infection with a MOI of 2.

For purification from bacterial as well as from insect cells, pellets were resuspended in buffer A (20 mM Hepes pH 7.5, 500 mM NaCl, 4 mM $MgCl_2$, 2 mM β-mercaptoethanol) and disrupted by sonication. The cell debris was removed by centrifugation at 20,000 g for 1 h at 4 °C and the recombinant proteins were purified by sequential Ni^{2+} (HisTrap excel; GE Healthcare; equilibrated in buffer A) and StrepII (Strep-Tactin XT Superflow; IBA; equilibrated in 25 mM Tris pH 8.0, 250 mM NaCl, 1 mM EDTA) affinity chromatography. The tags were cleaved-off by incubating the protein with TEV protease overnight at 4 °C. The cleaved tags and the protease were removed by an additional Ni^{2+} affinity chromatography step. The recombinant proteins were further purified by size exclusion chromatography at 4 °C on a HiLoad 16/600 Superdex 200 pg (GE Healthcare) equilibrated with 20 mM Hepes pH 7.5, 150 mM NaCl, 1 mM $MgCl_2$, 0.5 mM TCEP. Proteins concentrated to 15 mg/ml and snap frozen in liquid N_2. Molar protein concentrations were calculated using their molar extinction coefficient and the molecular masses for $BIR2^{289-605}$, $BIR2^{258-605}$, $SERK3^{250-615}$, $BRI1^{814-1196}$ of 35.3, 38.8, 41.5, 42.7 kDa, respectively.

Supplemental Figures

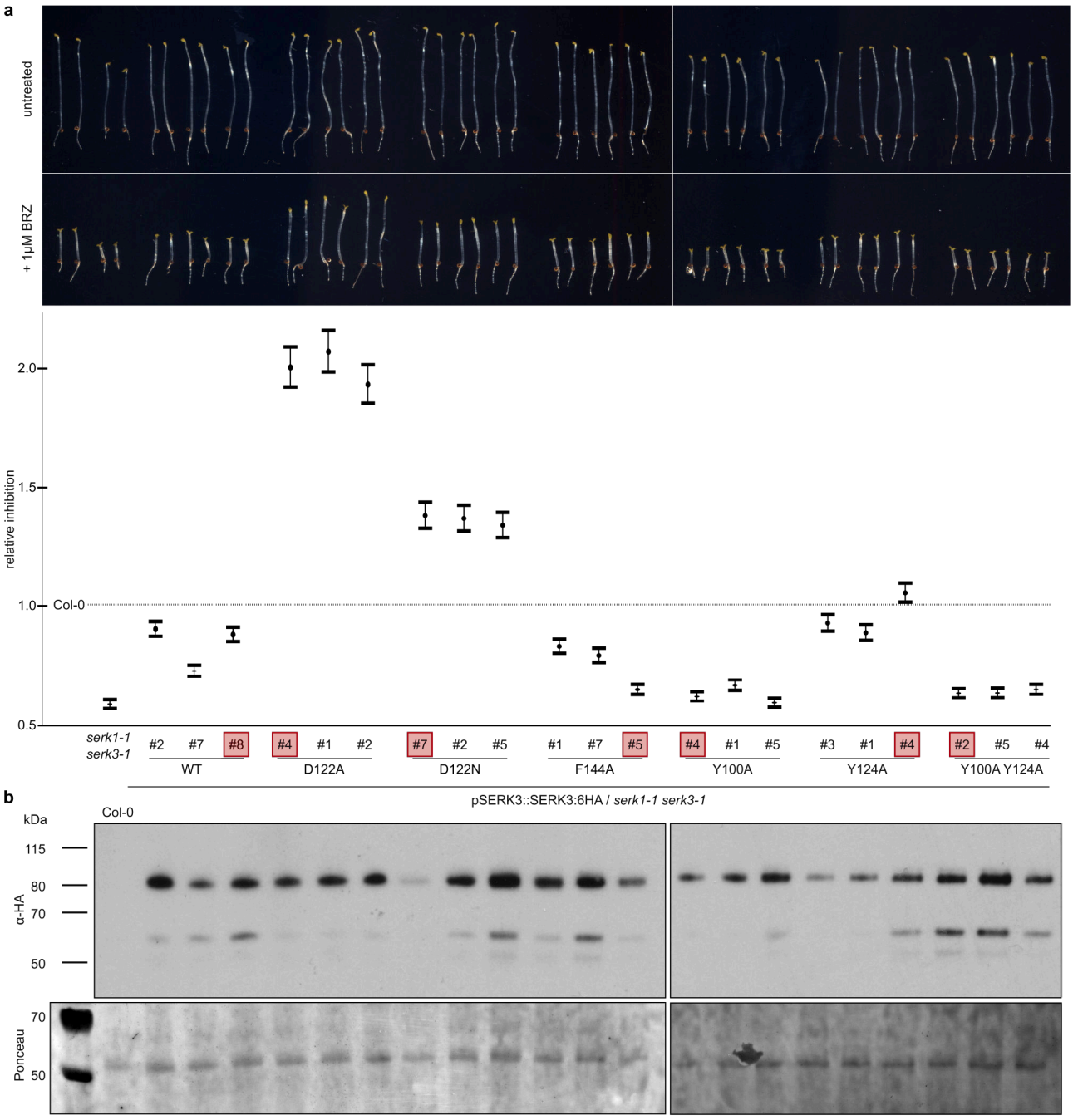

Supplementary Fig. 1: Hypocotyl growth assay with three independet lines for each transgenic line shown in Fig. 1b.

a, Hypocotyl growth assay of dark grown seedlings in the presence and absence of the BR biosynthesis inhibitor brassinazole (BRZ). Three independent lines are assessed for each construct, and the transgenic line shown in Figs. 1b,c and 4f is highlighted with a red box. Quantification of the data is shown beneath, plotting the relative inhibition and including the lower and upper confidence intervals. For each sample (i.e. genotype and treated or untreated) n=50 biologically independent hypocotyls, coming from 5 different ½MS plates, were measured.

b, Western blot using an HA antibody against SERK3:HA and using the plant material shown in (**a**). The Ponceau-stained membrane is shown as loading control below.

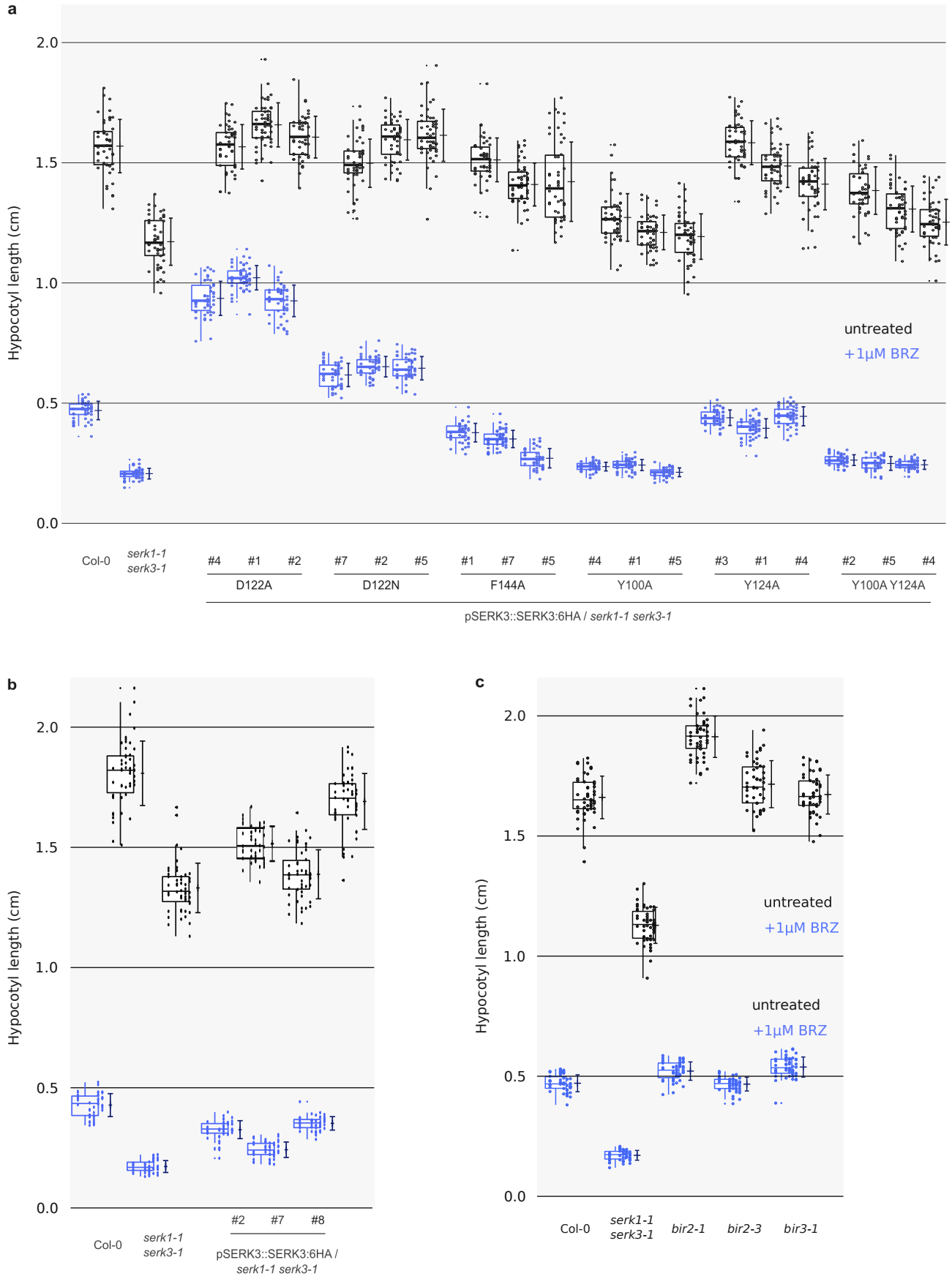

Supplementary Fig. 2: Hypocotyl growth assay raw data.

Shown are box plots (center line, median; box limits, upper and lower quartiles; whiskers, 1.5x interquartile range; points, outliers) with the raw data depicted as individual dots (grouped per plate) and mean ± standard deviation alongside. (**a,b**) Representation of the raw data for Fig. 1b, Supplementary Fig. 1 and (**c**) for Fig. 2c. Untreated: black, BRZ treated: blue. For each sample n=50 biologically independent hypocotyls, coming from 5 different ½MS plates, have been measured.

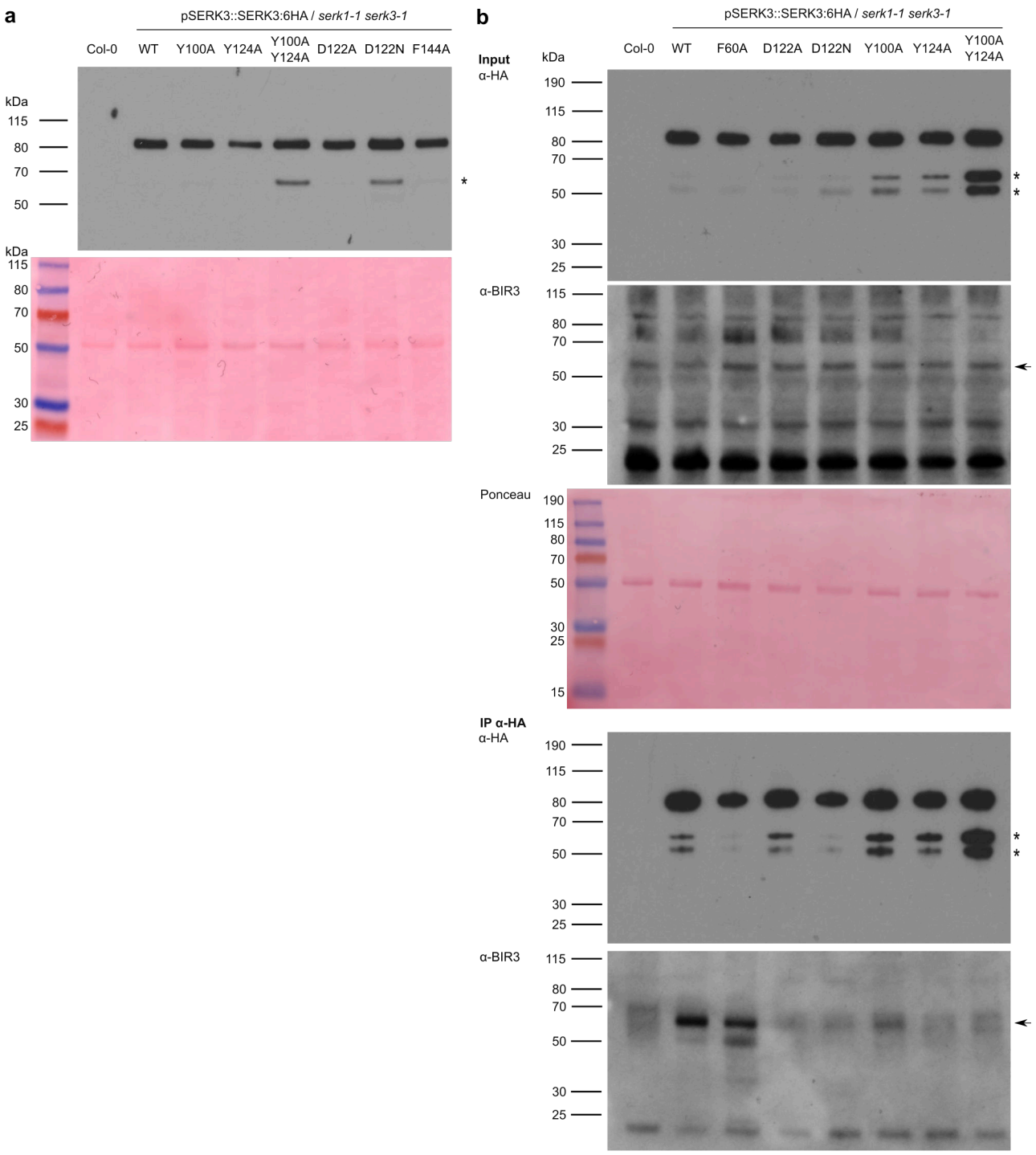

Supplementary Fig. 3: Full western blots and Ponceau stained membranes.

Scans of the full western blots and stained membranes used to prepare Fig. 1c (**a**) and Fig. 4f (**b**). Asterisks depict a truncated SERK3 protein and the arrows in (**b**) the BIR3 band.

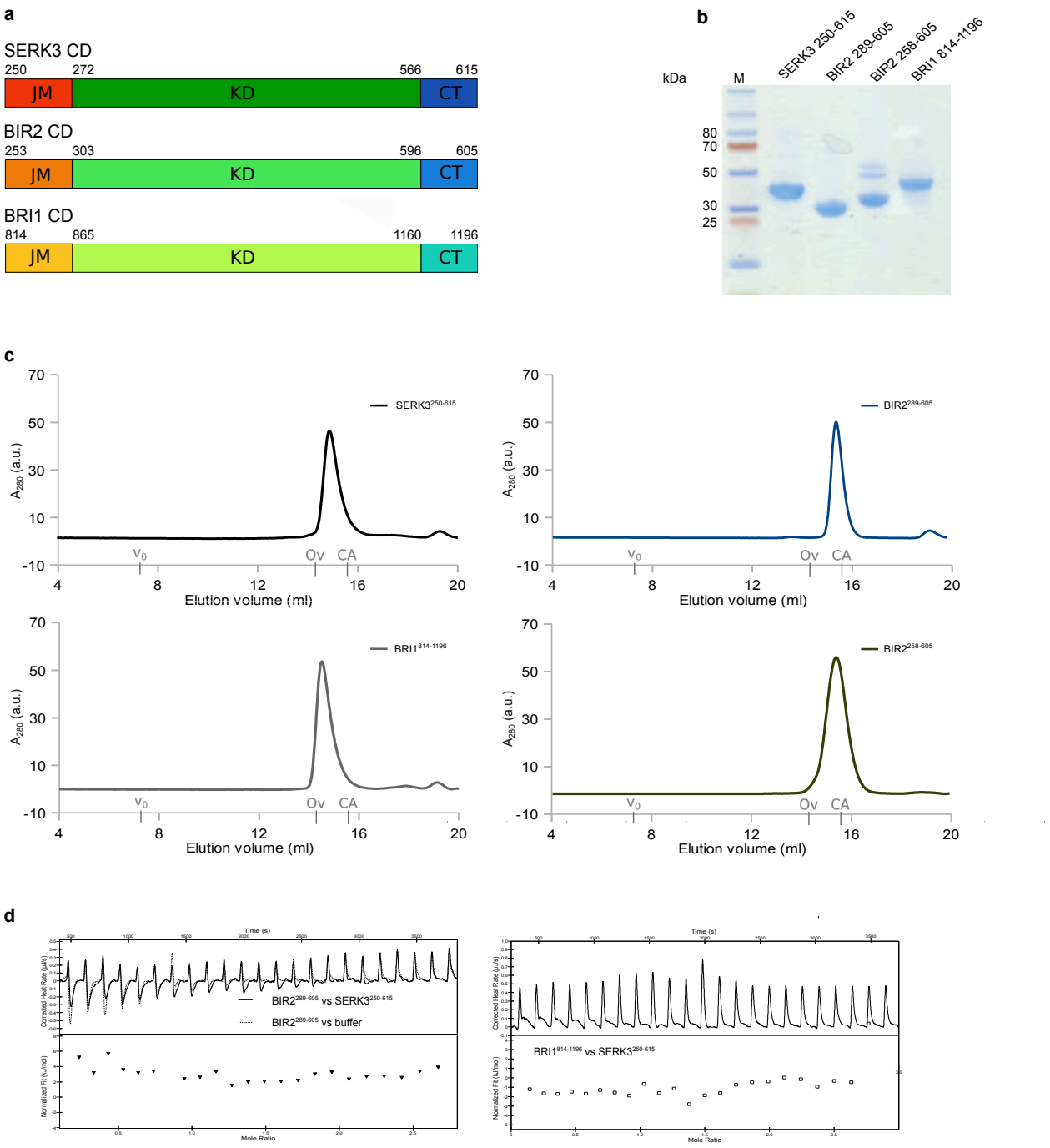

Supplementary Fig. 4: The recombinant BIR2 and SERK3 cytoplasmic domains do not interact *in vitro*.

a, Structural organization of the SERK3, BIR2 and BRI1 cytoplasmic domains (CD) with domain borders included. JM, juxtamembrane domain; KD, kinase domain; CT, C-terminal domain.

b,c, Analysis of the purified cytoplasmic domains on (**b**) a Coomassie stained 10 % SDS-PAGE gel and (**c**) by size exclusion chromatography on a Superdex 200 increase 10/300 GL column (GE Healthcare) reveals that all isolated cytoplasmic domains behave as apparent monomers in solution. The void (v_0) volume is shown, together with elution volumes for molecular mass standards (Ov, Ovalbumin, 44,000 Da; CA, Carbonic anhydrase, 29,000 Da).

d, Isothermal titration calorimetry (ITC) experiments with cytoplasmic domains of SERK3 vs. BIR2 (left) and BRI1 (right). No binding was detected, suggesting that the binding affinity between BIR2 and SERK3 or BRI1 and SERK3 is relatively low. Thus, BIR binding may be driven by their extracellular, rather than by their cytoplasmic domains.

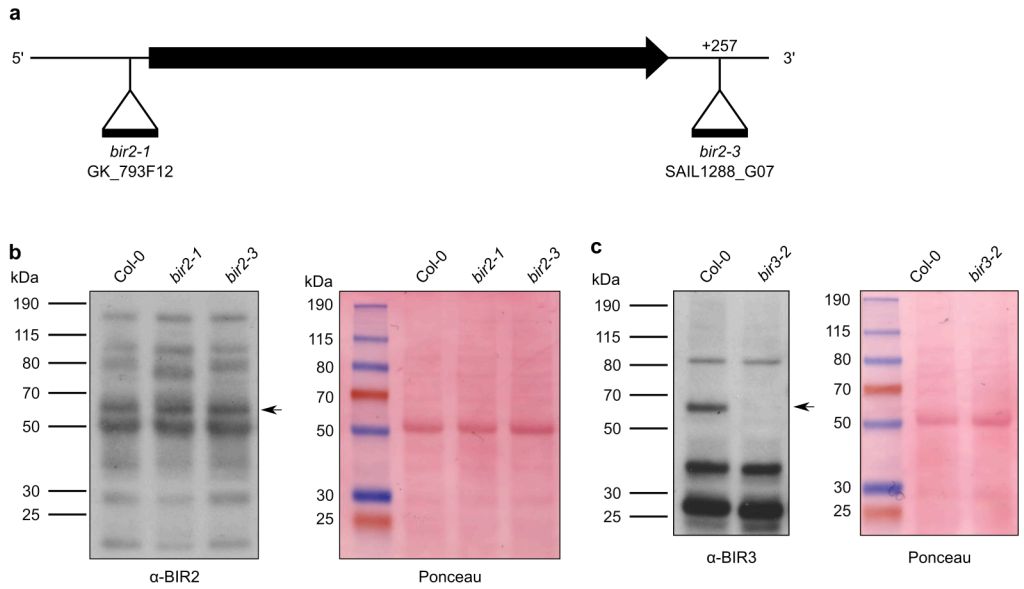

Supplementary Fig. 5: Expression levels of BIR2/3 in mutant lines.

a, Schematic overview of the T-DNA insertion sites *bir2-1*[2] and *bir2-3* (this study) shown as black triangles in the *BIR2* locus (bold black arrow). The T-DNA in *bir2-3* is inserted 257 bp downstream of the Stop codon.

b, Analysis of BIR2 protein levels in wild-type Col-0, *bir2-1* and *bir2-3* mutant plants. The position of the T-DNA insertion and the accumulation of BIR2 protein in these mutant lines, together suggest that both *bir2-1* and *bir2-3* cannot be considered null alleles. The arrow depicts the BIR2 band.

c, BIR3 protein levels in Col-0 and *bir3-2* (SALK_116632)[3] mutant lines. Ponceau stained membranes are shown alongside as loading controls. The arrow depicts the BIR3 band.

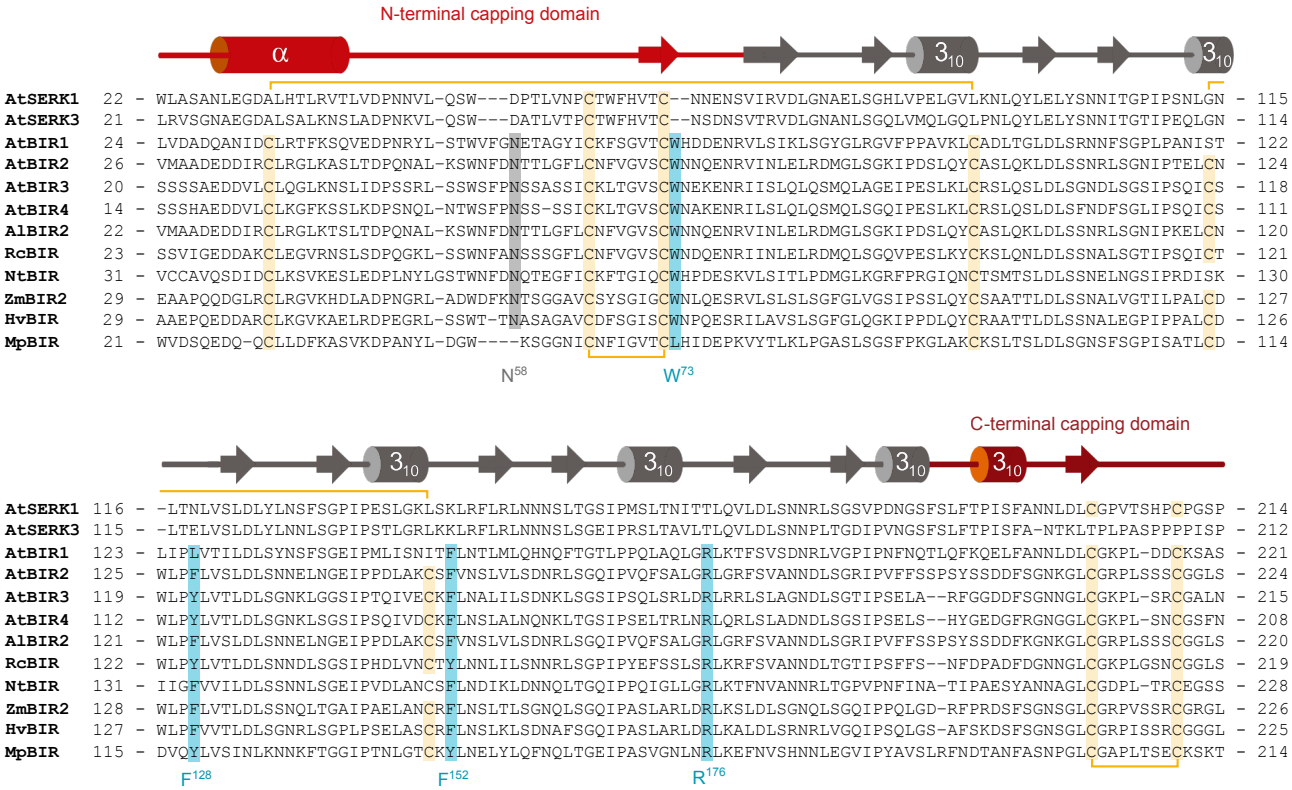

Supplementary Fig. 6: BIR – SERK complex interface residues are conserved among BIR family members from different species.

a, Structure based sequence alignment of the ectodomains of *Arabidopsis thaliana* SERK1 (Uniprot [http://www.uniprot.org] identifier: Q94AG2), SERK3 (Uniprot identifier: Q94F62), BIR1 (Uniprot identifier: Q9ASS4), BIR2 (Uniprot identifier: Q9LSI9), BIR3 (Uniprot identifier: O04567), BIR4 (Uniprot identifier: C0LGI5), *Arabidopsis lyrata* BIR2 (Uniprot identifier: D7LPU1), *Ricinus communis* BIR (Uniprot identifier: B9RUI5), *Nicotiana tabacum* BIR (Uniprot identifier: A0A1S4BB12), *Zea mays* BIR2 (Uniprot identifier: K7TUC5), *Hordeum vulgare* BIR (Uniprot identifier: F2E7N3) and *Marchantia polymorpha* BIR (Uniprot identifier: A7VM20). Shown alongside is a secondary structure assignment, with the N- and C-terminal capping domains highlighted in red, calculated using DSSP[23]. BIR residues of the lateral protein interaction interface are highlighted in blue, disulfide bridges in yellow and the conserved N-terminal glycosylation site in gray. All numbering refers to AtBIR2.

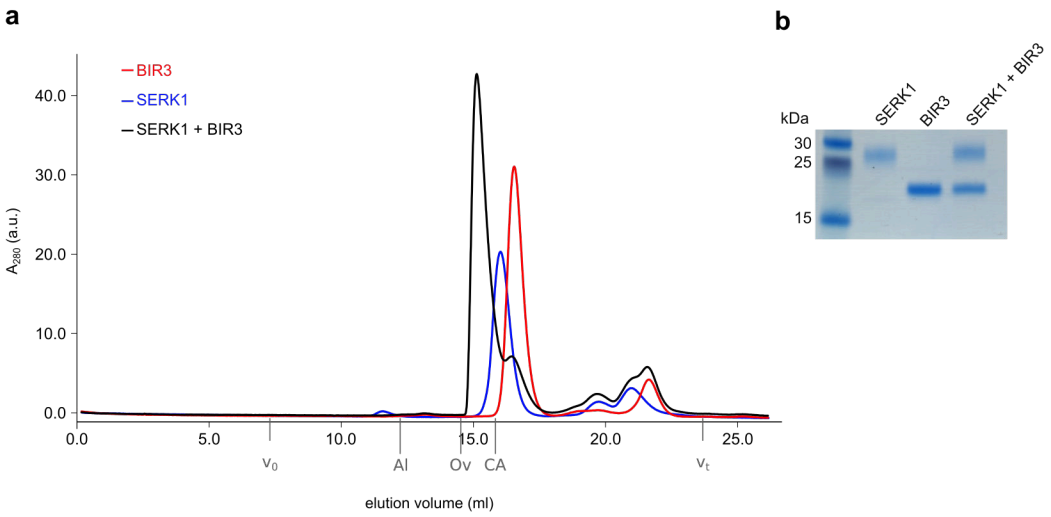

Supplementary Fig. 7: The BIR3 and SERK1 ectodomains form heterodimers in solution.

a,b, Analytical size exclusion chromatography. The isolated BIR3 (red absorption trace) and SERK3 (blue) ectodomains elute as apparent monomers when run in isolation, and form a heterodimeric complex (black line). Void (v_0) volume and total volume (v_t) are shown, together with elution volumes for molecular mass standards (Al, Aldolase, 158,000 Da; Ov, Ovalbumin, 44,000 Da; CA, Carbonic anhydrase, 29,000 Da). A SDS PAGE analysis of the peak fractions is shown in (**b**).

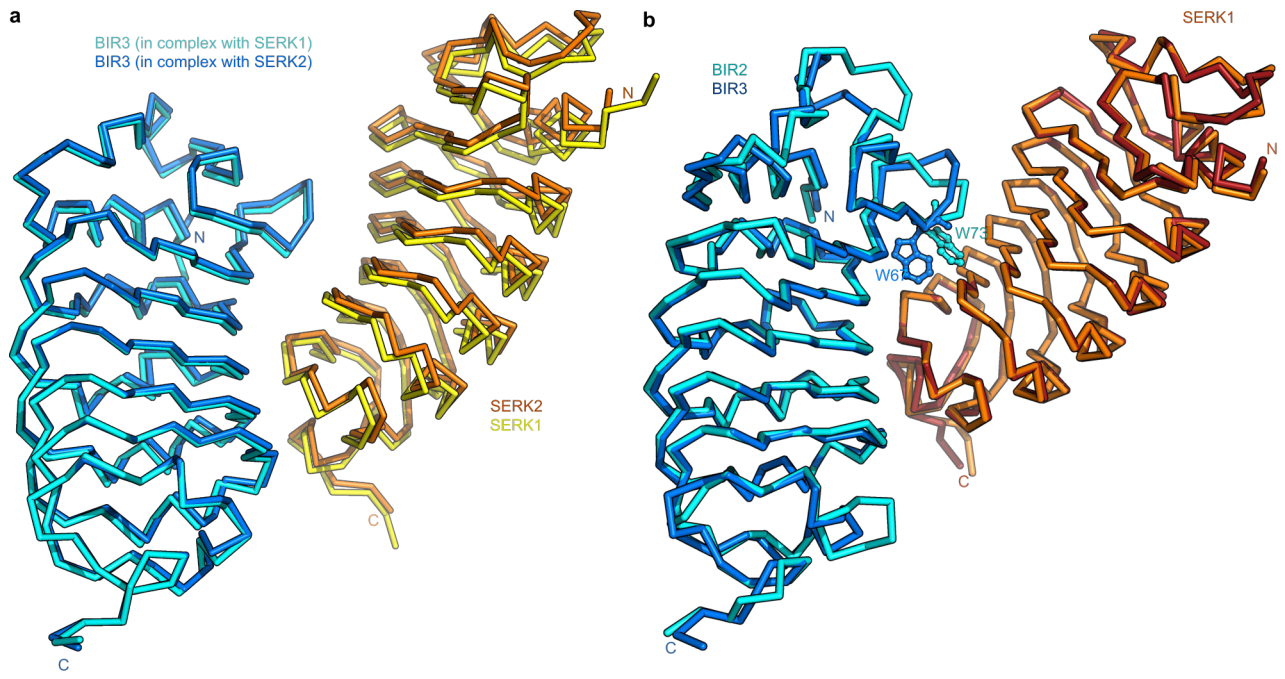

Supplementary Fig. 8: Different BIR – SERK complexes are highly similar and no major conformational changes occur upon BIR3 – SERK1 complex formation.

a, Structural superposition of the BIR3 – SERK1 and the BIR3 – SERK2 complex (r.m.s.d. is ~1.8 Å comparing 316 corresponding C_α atoms). Shown are C_α traces of SERK1 (yellow) and SERK2 (orange) as seen in complex with BIR3 (cyan / blue respectively).

b, Structural superposition of the BIR3 – SERK1 complex with the isolated BIR2 (r.m.s.d. is ~1.2 Å comparing 160 corresponding C_α atoms) and SERK1 (PDB-ID 4LSC[19], r.m.s.d. is ~0.9 Å comparing 186 corresponding C_α atoms) ectodomains. Shown are C_α traces of SERK1 (orange for the isolated ectodomain and red for SERK1 in complex with BIR3), BIR2 (in cyan) and BIR3 (in blue). $BIR3^{W67}$ and the corresponding $BIR2^{W73}$ are highlighted as ball-and-sticks.

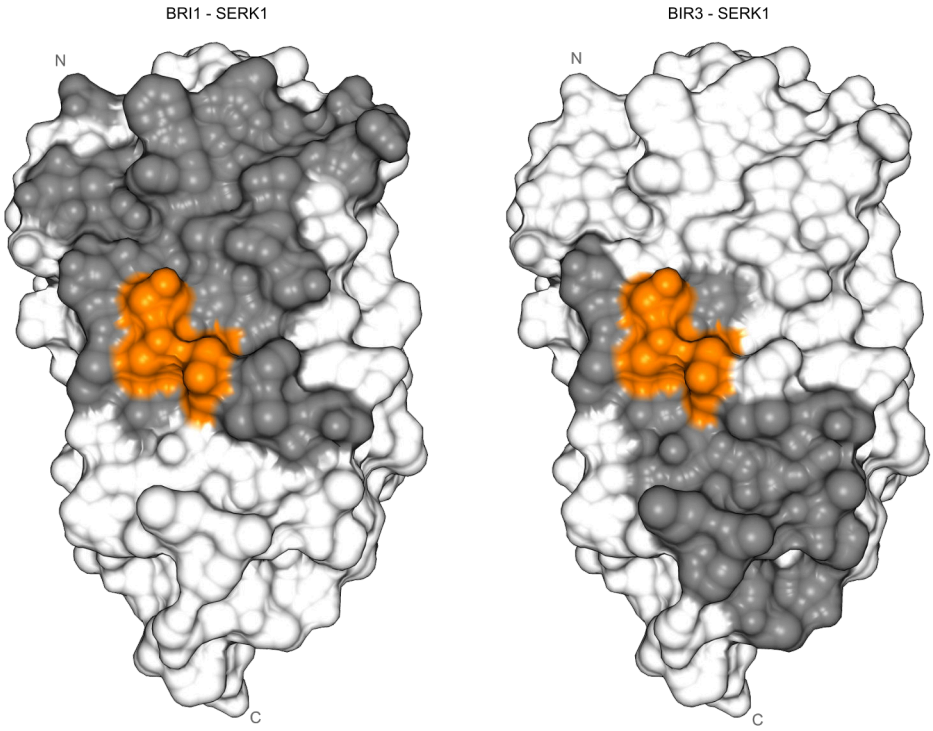

Supplementary Fig. 9: Partly overlapping surface areas in SERK1 are involved in BRI1 and BIR3 binding, respectively.

Surface view of the SERK1 ectodomain with BRI1 (left) and BIR3 (right) interacting residues (defined using the program PISA[24]) shown in dark gray. Interaction with BRI1 involves mainly residues originating from the SERK1 N-terminal cap, while the interaction with BIR3 involves residues from the two C-terminal LRRs and from the C-terminal cap. Importantly, the *elg* mutation and the corresponding SERK3^{D122} forms part of both complex interfaces (highlighted in orange).

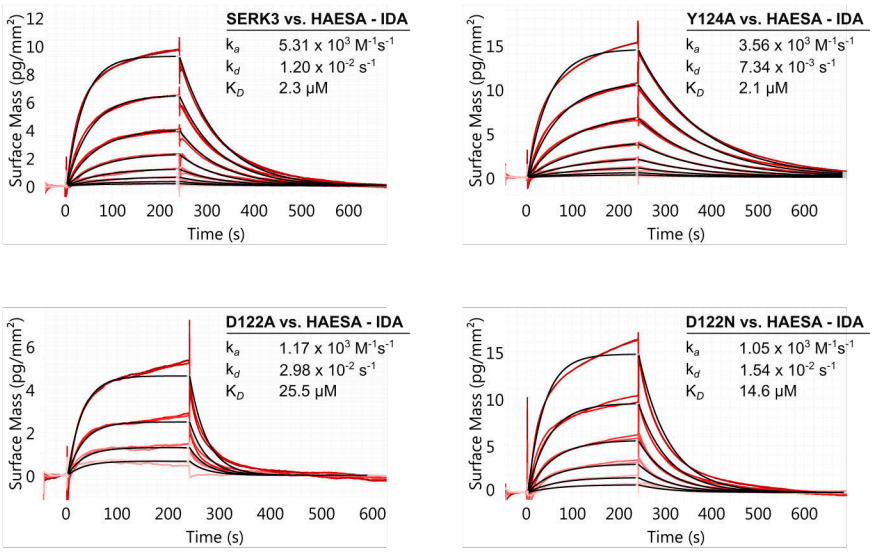

Supplementary Fig. 10: SERK3D122A and D122N disrupt interaction with the LRR-RK HAESA

Binding kinetics for SERK3, SERK3^{Y124A}, SERK3^{D122A} and SERK3^{D122N} (*elg*) vs. HAESA in the presence of the peptide ligand IDA obtained from grating-coupled interferometry (GCI) experiments. Sensograms with recorded data are shown in red with the respective fits in black, and include table summaries of the corresponding association rate constant (k_a), dissociation rate constant (k_d) and dissociation constant K_D.

The SERK3^{D122A} and SERK3^{D122N} ectodomain bind the HAESA LRR domain with reduced binding affinity when compared to wild-type SERK3 (~10 fold and ~6 fold, respectively). This is in contrast to BRI1, which binds these mutant proteins with wild type-like affinity (compare Fig. 1d). The pronounced and BR-specific gain-of-function effect of SERK elg mutants could thus be due to the fact that the mutant co-receptor can still activate BRI1 but cannot form signaling competent complexes with other LRR-RKs. This would increase the pool-size of a SERK3 variant that is both available for BR signaling and not under negative regulation by BIRs. It is of note that SERK3^{Y124A}, which also disrupts interactions with BIRs (Fig. 4d) still binds BRI1 – BL and HAESA-IDA with wild-type affinity. Thus SERK3^{Y124A} may still be able to interact with many different LRR-RKs, limiting the co-receptor pool size available to BRI1. Consistently, this mutant shows only a very moderate gain-of-function phenotype *in vivo* (Fig. 1b).

Supplementary Table 1: Statistical evaluation of the hypocotyl growth assays

		relative Inhibition	Lower CI	Upper CI
serk1-1, 3-1 / Col-0		0.588	0.561	0.615
SERK3WT / Col-0	#2	0.902	0.863	0.943
	#7	0.727	0.696	0.759
	#8	0.879	0.842	0.919
Y100A / Col-0	#1	0.619	0.592	0.649
	#4	0.667	0.637	0.699
	#5	0.594	0.567	0.622
Y124A / Col-0	#1	0.927	0.885	0.971
	#3	0.887	0.847	0.929
	#4	1.054	1.007	1.104
Y100A ,Y124A / Col-0	#2	0.634	0.605	0.664
	#4	0.634	0.606	0.664
	#5	0.649	0.620	0.680
D122A / Col-0	#1	1.999	1.909	2.094
	#2	2.065	1.972	2.163
	#4	1.928	1.841	2.019
D122N / Col-0	#2	1.378	1.317	1.443
	#5	1.366	1.305	1.430
	#7	1.337	1.278	1.400
F144A / Col-0	#1	0.830	0.793	0.869
	#5	0.832	0.794	0.871
	#7	0.634	0.605	0.664
bir2-1 / Col-0		0.962	0.925	0.999
bir2-3 / Col-0		0.962	0.927	0.998
bir3-2 / Col-0		1.134	1.092	1.179

Relative inhibition and confidence intervals (CI) are calculated based on the raw data shown in Supplementary Fig. S2. For each sample (i.e. genotype and treated or untreated) n=50 biologically independent hypocotyls, coming from 5 different ½MS plates, have been measured.

Supplementary Table 2. Data collection, phasing and refinement statistics

	BIR2 *sulfur SAD*[*]	**BIR2** *native*[*]	**BIR3 – SERK1** *native*[*]	**BIR3 – SERK2** *native*[*]
Data collection				
Space group	$P6_422$	$P6_422$	$P2_1$	$P2_12_12_1$
Cell dimensions				
a, *b*, *c* (Å)	153.77, 153.77, 110.06	153.77, 153.77, 110.06	52.17, 50.76, 77.43	50.18, 52.15, 308.89
α, β, γ (°)	90, 90, 120	90, 90, 120	90, 96.72, 90	90, 90, 90
Resolution (Å)	44.75 – 3.0 (3.08 – 3.0)	45.77 – 1.90 (2.02 – 1.90)	40.81 – 1.25 (1.33 – 1.25)	49.41 – 2.20 (2.33 – 2.20)
R_{meas}[#]	0.229 (1.00)	0.221 (2.88)	0.058 (1.10)	0.115 (1.67)
$I/\sigma I$[#]	35.50 (7.69)	11.90 (1.0)	15.1 (1.5)	17.0 (1.4)
Completeness (%)[#]	100.0 (99.8)	100.0 (97.9)	99.8 (95.5)	99.9 (99.7)
Redundancy[#]	121.9 (121.4)	13.15 (12.8)	6.3 (5.7)	13.0 (13.0)
Refinement				
Resolution (Å)		45.77 – 1.90	40.81 – 1.25	49.41 – 2.20
No. reflections		57,323	104,302	40,314
R_{work}/ R_{free}[$]		0.21/0.23	0.15/0.18	0.22/0.25
No. atoms				
protein		2,986	2,962	5,639
glycan		59	165	162
PEG			44	14
solvent		120	433	141
Res. B-factors[$]				
protein		37.4	21.1	62.9
glycan		54.6	65.4	90.9
PEG			44.8	65.4
solvent		36.7	39.2	51.3
R.m.s deviations[$]				
Bond lengths (Å)		0.008	0.012	0.010
Bond angles (°)		1.34	1.61	1.43
PDB - ID		**6FG7**	**6FG8**	**6G3W**

[#]as defined XDS[11] or [$]in Refmac5[17], respectively. [*]Data were collected from one crystal per experiment.

Supplementary Table 3: Primers used in this study

Primer name	Sequence
SERK3prom-attB4	GGGGACAACTTTGTATAGAAAAGTTGCTTGTTTTTTGGAAACAGAG
SERK3prom-attB1R	GGGGACTGCTTTTTTGTACAAACTTGCTTTATCCTCAAGAGATTA
SERK3-attB1	GGGGACAAGTTTGTACAAAAAAGCAGGCTTAACCATGGAACGAAGATTAATGATCCC
SERK3noSTOP-attB2	GGGGACCACTTTGTACAAGAAAGCTGGGTATCTTGGACCCGAGGGGTATT
SDM-fwSERK3_F60A	CATGGGCTCATGTTACTTGCAATAGCGACAATAGTGTTACACG
SDM-rvSERK3_F60A	AGTAACATGAGCCCATGTACATGGAGTAACAAGAGTAGCATCCC
SDM-fwSERK3_H61A	CATGGTTTGCTGTTACTTGCAATAGCGACAATAGTGTTACACG
SDM-rvSERK3_H61A	AGTAACAGCAAACCATGTACATGGAGTAACAAGAGTAGCATCCC
SDM-fwSERK3_H61A-F60A	CATGGGCTGCTGTTACTTGCAATAGCGACAATAGTGTTACACG
SDM-rvSERK3_H61A-F60A	AGTAACAGCAGCCCATGTACATGGAGTAACAAGAGTAGCATCCC
SDM-fwSERK3_Y100A	AGGGAGCTTGCTAGCAATAACATTACTGGGACAATCCCAG
SDM-rvSERK3_Y100A	GCTAGCAAGCTCCCTGTCATTACCATTCTTTAATATTAATTTC
SDM-fwSERK3_Y100A-cds	GGAGCTTGCTAGCAATAACATTACTGGGACAATCCCAG
SDM-rvSERK3_Y100A-cds	GTTATTGCTAGCAAGCTCCAAGTACTGCAAGTTTGGAAGC
SDM-fwSERK3_Y124A	GATCTTGCCTTGAACAATTTAAGCGGGCCTATTCCATCAAC
SDM-rvSERK3_Y124A	GTTCAAGGCAAGATCCAAGCTCACCAATTCCGTCAGATTTCC
SDM-fwSERK3_F144A	CTCCGTGCCTTGTATGCACCATATTCTACTCTCTTCTTTTAATAC
SDM-rvSERK3_F144A	GCATACAAGGCACGGAGTTTCTTAAGTCGGCCGAGAGTTG
SDM-fwSERK3_F144A-cds	CTCCGTGCCTTGCGTCTTAATAACAATAGCTTATCTGGAG
SDM-rvSERK3_F144A-cds	GACGCAAGGCACGGAGTTTCTTAAGTCGGCCGAGAGTTG
SDM-fwSERK3_R146A	GGTTAGGGCTCTTAATAACAATAGCTTATCTGGAGAAAT
SDM-rvSERK3_R146A	TATTAAGAGCCCTAACCACCAATACAAAAAGAGAATGTC
SDM-fwSERK3_R146A-cds	GTTTCTTGGCTCTTAATAACAATAGCTTATCTGGAGAAAT
SDM-rvSERK3_R146A-cds	TATTAAGAGCCAAGAAACGGAGTTTCTTAAGTCGGCCG
SDM-fwBIR2co_W73A	GTCCTGC GCG AACAACCAGGAAAACCGCGTCATC
SDM-rvBIR2co_W73A	GTTGTT CGC GCAGGACACGCCCACGAAGTTGCAGAG
SDM-fwBIR2co_R79A	GAGAAT GCG GTTATCAATCTTGAGCTTCGTGATATG
SDM-rvBIR2co_R79A	GATAAC CGC ATTCTCCTGATTGTTCCAACAAGACAC
SDM-fwBIR2co_E84R	CAATCTT CGG CTTCGTGATATGGGTTTATCTGGTAAA
SDM-rvBIR2co_E84R	CACGAAG CCG AAGATTGATAACCCTATT CTC CTGATTG
SDM-fwBIR2co_F152A	GTGTAGC GCT GTGAATTCTTTGGTTTTGTCTGATAAC
SDM-rvBIR2co_F152A	ATTCAC CGA GCTACACTTAGCTAAATCAGGAGGAATC
SDM-fwBIR2co_V157D	TCTTTG GAT TTGTCTGATAACCGGCTTTCGGGTCAAA
SDM-rvBIR2co_V157D	CAGACAA ATC CAAAGAATTCACAAAGC TAC ACTTAGC
SDM-fwBIR2co_R176A	TTAGGG GCG TTAGGGAGGTTCTCTGTTGCTAATAATG
SDM-rvBIR2co_R176A	CCCTAA CGC CCCTAAAGCCGAGAACTGAACCGGGATT
BIR2_1-222_Gfw	ATTCATACCGTCCCACCATCGGGCGCGG ATGAAAGAGATCGGCTCAAAACC
BIR2_1-222_Grv	CAAGCACCCTGGAAGTACAGGTT CTCGAG ACCACCACAACTCGAAGATAA
BIR3_1-213_Gfw	ATTCATACCGTCCCACCATCGGGCGCGG ATGAAGAAGATCTTCATCAC
BIR3_1-213_Grv	CAAGCACCCTGGAAGTACAGGTTCTCGAG CGCTCCACATCGCGATAAAGG
SERK3_1-220_Gfw	ATTCATACCGTCCCACCATCGGGCGCGG ATGGAACGAAGATTAATGATCC
SERK3_1-220_Grv	CAAGCACCCTGGAAGTACAGGTTCTCGAG ACTCCCTGCAGGTGATGG

SDM, primer used for site directed mutagenesis; rv, revers; fw, forward; G, primer used for Gibson cloning

References

1. Clough, S. J. & Bent, A. F. Floral dip: a simplified method forAgrobacterium-mediated transformation ofArabidopsis thaliana. *Plant J.* **16,** 735–743 (1998).
2. Halter, T. *et al.* The Leucine-Rich Repeat Receptor Kinase BIR2 Is a Negative Regulator of BAK1 in Plant Immunity. *Curr. Biol.* **24,** 134–143 (2014).
3. Imkampe, J. *et al.* The Arabidopsis Leucine-Rich Repeat Receptor Kinase BIR3 Negatively Regulates BAK1 Receptor Complex Formation and Stabilizes BAK1. *Plant Cell* **29,** 2285–2303 (2017).
4. Albrecht, C., Russinova, E., Kemmerling, B., Kwaaitaal, M. & de Vries, S. C. Arabidopsis SOMATIC EMBRYOGENESIS RECEPTOR KINASE proteins serve brassinosteroid-dependent and -independent signaling pathways. *Plant Physiol.* **148,** 611–619 (2008).
5. Russinova, E. *et al.* Heterodimerization and endocytosis of Arabidopsis brassinosteroid receptors BRI1 and AtSERK3 (BAK1). *Plant Cell* **16,** 3216–3229 (2004).
6. Schindelin, J. *et al.* Fiji: an open-source platform for biological-image analysis. *Nat. Methods* **9,** 676–682 (2012).
7. Kitsche, A. & Hothorn, L. A. Testing for qualitative interaction using ratios of treatment differences. *Stat. Med.* **33,** 1477–1489 (2014).
8. Hothorn, T., Bretz, F. & Westfall, P. Simultaneous inference in general parametric models. *Biom. J.* **50,** 346–363 (2008).
9. R Core Team. *R: A language and environment for statistical computing. R Foundation for Statistical Computing, Vienna, Austria. 2013*. (ISBN 3-900051-07-0, 2014).
10. Nuzzo, R. Scientific method: statistical errors. *Nature* **506,** 150–152 (2014).
11. Kabsch, W. Automatic processing of rotation diffraction data from crystals of initially unknown symmetry and cell constants. *J. Appl. Crystallogr.* **26,** 795–800 (1993).
12. Sheldrick, G. M. A short history of SHELX. *Acta Crystallogr. A* **64,** 112–122 (2008).
13. Adams, P. D. *et al.* PHENIX: a comprehensive Python-based system for macromolecular structure solution. *Acta Crystallogr. D Biol. Crystallogr.* **66,** 213–221 (2010).

14. Bricogne, G., Vonrhein, C., Flensburg, C., Schiltz, M. & Paciorek, W. Generation, representation and flow of phase information in structure determination: recent developments in and around SHARP 2.0. *Acta Crystallogr. D Biol. Crystallogr.* **59,** 2023–2030 (2003).
15. Terwilliger, T. C. SOLVE and RESOLVE: automated structure solution and density modification. *Methods Enzymol.* **374,** 22–37 (2003).
16. Emsley, P. & Cowtan, K. Coot: model-building tools for molecular graphics. *Acta Crystallogr. D Biol. Crystallogr.* **60,** 2126–2132 (2004).
17. Murshudov, G. N., Vagin, A. A. & Dodson, E. J. Refinement of macromolecular structures by the maximum-likelihood method. *Acta Crystallogr. D Biol. Crystallogr.* **53,** 240–255 (1997).
18. McCoy, A. J. *et al.* Phaser crystallographic software. *J. Appl. Crystallogr.* **40,** 658–674 (2007).
19. Santiago, J., Henzler, C. & Hothorn, M. Molecular mechanism for plant steroid receptor activation by somatic embryogenesis co-receptor kinases. *Science* **341,** 889–892 (2013).
20. Wang, J. *et al.* Allosteric receptor activation by the plant peptide hormone phytosulfokine. *Nature* **525,** 265–268 (2015).
21. Davis, I. W. *et al.* MolProbity: all-atom contacts and structure validation for proteins and nucleic acids. *Nucleic Acids Res.* **35,** W375-383 (2007).
22. Pettersen, E. F. *et al.* UCSF Chimera--a visualization system for exploratory research and analysis. *J. Comput. Chem.* **25,** 1605–1612 (2004).
23. Kabsch, W. & Sander, C. Dictionary of protein secondary structure: pattern recognition of hydrogen-bonded and geometrical features. *Biopolymers* **22,** 2577–2637 (1983).
24. Krissinel, E. & Henrick, K. Inference of macromolecular assemblies from crystalline state. *J. Mol. Biol.* **372,** 774–797 (2007).